The emergence of a stable neuronal ensemble from a wider pool of activated neurons in the dorsal medial prefrontal cortex during appetitive learning in mice

Article (Accepted Version)

Title: The emergence of a stable neuronal ensemble from a wider pool of activated neurons in the dorsal medial prefrontal cortex during appetitive learning in mice

Abbreviated Title: Cortical appetitive neuronal ensemble formation

Authors: Leonie S. Brebner[†1], Joseph J. Ziminski[†1], Gabriella Margetts-Smith[1,7], Meike C. Sieburg[1,8], Hayley M. Reeve[1], Thomas Nowotny[2], Johannes Hirrlinger[3], Tristan G. Heintz[4], Leon Lagnado[4], Shigeki Kato[5], Kazuto Kobayashi[5], Leslie A. Ramsey[6], Catherine N. Hall[1], Hans S. Crombag[†1], Eisuke Koya[†*1]
†These authors contributed equally to this work.

Affiliation: [1]Sussex Neuroscience, School of Psychology, University of Sussex, Falmer, BN1 9QG; United Kingdom;
[2]Sussex Neuroscience, School of Engineering and Informatics, University of Sussex, Falmer, BN1 9QJ, United Kingdom;
[3]Carl-Ludwig-Institute for Physiology, University of Leipzig, Leipzig, Germany; and Department of Neurogenetics, Max-Planck-Institute for Experimental Medicine, Göttingen, Germany;
[4]Sussex Neuroscience, School of Life Sciences, University of Sussex, Falmer, BN1 9QG, United Kingdom;
[5]Department of Molecular Genetics, Institute of Biomedical Sciences, Fukushima Medical University School of Medicine, Fukushima 960-1295, Japan.
[6]Behavioral Neuroscience Branch, IRP/NIDA/NIH/DHHS, 251 Bayview Blvd, Suite 200, Baltimore, MD 21224., Baltimore, MD 21224, United States of America.

[*]Corresponding author:
Dr. Eisuke Koya
Sussex Neuroscience
School of Psychology
University of Sussex
Falmer, BN1 9QG, United Kingdom
Tel: +44-1273-877-776
E-mail: e.koya@sussex.ac.uk

Text information:
Number of pages including tables, figure and table legends, and references: 46 pages
Number of figures: 8
Number of tables: 2
Abstract: 239 words
Introduction: 623 words
Discussion: 1,492 words

Conflict of interest: The authors declare no competing financial interests.

[7]Current address: University of Exeter College of Medicine and Health, Hatherly Laboratories, Prince of Wales Road, Exeter EX4 4PS, United Kingdom.
[8]Current address: Department of Biomedicine/DANDRITE, Aarhus University, 8000 Aarhus C, Denmark

Acknowledgments: We thank Prof. William Wisden (Imperial College, UK) for providing the initial AAV2-TREtight-hM3Dq sample for the DREADD pilot experiments. Also, we thank Dr. Marsha Sindarto (University of Sussex, UK) for providing helpful advice with the generation of the aforementioned viruses and Nagisa Sawada (Fukushima Medical University, Japan) for providing assistance with AAV generation. We thank Alex Hoffman (NIDA IRP, USA) for providing helpful advice regarding the paired recording experiments, Bruce Hope (NIDA IRP, USA) for providing additional *Fos-GFP* mice brains for analysis, and Nobuyoshi Suto (Scripps Research, USA) for helpful comments with the manuscript.

Support: This research was supported by the Biotechnology and Biological Sciences Research Council (BBSRC) grant number BB/M009017/1, MRC Discovery Award, The University of Sussex Strategic Development Funds, Sussex Neuroscience 4-year PhD programme, and the Intramural Research Program, National Institute on Drug Abuse, National Institutes of Health.

Abstract

Animals selectively respond to environmental cues associated with food reward to optimize nutrient intake. Such appetitive CS-US associations are thought to be encoded in select, stable neuronal populations or neuronal ensembles, which undergo physiological modifications during appetitive conditioning. These ensembles in the medial prefrontal cortex (mPFC) control well-established, cue-evoked food seeking, but the mechanisms involved in the genesis of these ensembles are unclear. Here, we utilized **male** *Fos-GFP* mice that express the green fluorescent protein (GFP) in recently behaviorally-activated neurons, to reveal how dorsal mPFC neurons are recruited and modified to encode CS-US memory representations using an appetitive conditioning task. In the initial conditioning session, animals did not exhibit discriminated, cue-selective food seeking, but did so in later sessions indicating that a CS-US association was established. Using microprism-based *in vivo* 2-Photon imaging, we revealed that only a minority of neurons activated during the initial session was consistently activated throughout subsequent conditioning sessions and during cue-evoked memory recall. Notably, using *ex vivo* electrophysiology we found that neurons activated following the initial session exhibited transient hyper-excitability. Chemogenetically enhancing the excitability of these neurons throughout subsequent conditioning sessions interfered with the development of reliable cue-selective food seeking, indicated by persistent, non-discriminated performance. We demonstrate how appetitive learning consistently activates a subset of neurons to form a stable neuronal ensemble during the formation of a CS-US association. This ensemble may arise from a pool of hyper-excitable neurons activated during the initial conditioning session.

Significance statement

Appetitive conditioning endows cues associated with food with the ability to guide food-seeking, through the formation of a food-cue association. Neuronal ensembles in the medial prefrontal cortex (mPFC) control established cue-evoked food-seeking. However, how neurons undergo physiological modifications and become part of an ensemble during conditioning remain unclear. We found that only a minority of dorsal mPFC (dmPFC) neurons activated on the initial conditioning session became consistently activated during conditioning and memory recall. These initially activated neurons were also transiently hyper-excitable. We demonstrate: 1) how stable neuronal ensemble formation in the dmPFC underlies appetitive conditioning; and 2) how this ensemble may arise from hyper-excitable neurons activated prior to the establishment of cue-evoked food seeking.

Introduction

Through Pavlovian associative learning, a conditioned stimulus (or CS) that reliably predicts food reward (unconditioned stimulus or US) is endowed with motivational significance and the ability to activate and retrieve food memories (van den Akker et al., 2018; Jansen, 1998; Pavlov, 1927). These CS-activated food representations can elicit actions to facilitate food procurement. For animals, this maximizes caloric intake while minimizing time and energy spent searching for food (Carthey et al., 2011; MacArthur and Pianka, 1966). In humans, food-associated cues can elicit food cravings and produce eating in the absence of hunger, which may contribute to eating disorders involving binge eating (van den Akker et al., 2018; Jansen, 1998). Elucidating the neurobiological mechanisms underlying the establishment of appetitive CS-US associations is important for understanding both adaptive and maladaptive eating (van den Akker et al., 2018; Jansen, 1998).

The motivational functions of CS-activated memory representations involve activation of sparse sets of neurons or 'neuronal ensembles' in the medial prefrontal cortex (mPFC); a brain region implicated in various appetitive behaviors (Cruz et al., 2013; Koya et al., 2009; Riga et al., 2014; Suto et al., 2016; Whitaker and Hope, 2018). Accordingly, selective silencing of mPFC ensembles attenuates cue-evoked food-seeking (Suto et al., 2016). These findings offer compelling evidence that CS-activated mPFC ensembles stably encode associative memories that elicit and guide appetitive performance. The establishment of an appetitive CS-US association is readily examined using a Pavlovian conditioning task. In the initial conditioning sessions, animals do not exhibit discriminated cue-evoked food seeking, but in later sessions this behavior becomes more discriminated, indicating an establishment of a CS-US association (Ziminski et al., 2017). However, we have yet to understand how CS-US encoding neuronal ensembles are formed as these associations become established, i.e. as a function of conditioning.

We addressed this issue here by visualizing ensemble formation and activation patterns across conditioning sessions utilizing microprism-based 2-Photon (2P) *in vivo* imaging (Low et al., 2014). Unlike conventional cranial window 2P imaging, using a microprism allowed us to access the mPFC. We focused on the anterior cingulate cortex region of the dorsal mPFC (dmPFC) because it plays a

role in facilitating attentional processes and discriminating between food-predictive and non-predictive cues (Bryden et al., 2011; Cardinal et al., 2002; Parkinson et al., 2000; Totah et al., 2009). Furthermore, we crossed *Fos-GFP* and *GAD-tdTomato* mice to generate *Fos-GFP* X *GAD-TdTomato (FGGT)* mice. These mice express GFP in recently behaviorally-activated (GFP+) neurons with a similar time course to the acute neuronal activity marker 'Fos' (Barth et al., 2004; Whitaker et al., 2016; Ziminski et al., 2017). Also, they express the red fluorescent protein 'tdTomato' in interneurons (Besser et al., 2015). This enabled us to selectively track activation patterns of pyramidal cells (tdTomato–) and interneurons (tdTomato+) across learning and recall sessions in mice trained on a Pavlovian appetitive conditioning task.

Physiological adaptations in CS-activated ensembles are thought to play a role in establishing associative memories; changes in appetitive associative strength modulate ensemble excitability (Whitaker et al., 2017; Ziminski et al., 2017), while the formation of an appetitive association induces synaptic remodeling in an ensemble-specific manner (Whitaker et al., 2016). Similarly, fear conditioning studies have identified a critical role of increased synaptic strength and connectivity between learning-activated neurons in the establishment of aversive associative memories (Choi et al., 2018; Ryan et al., 2015). However, we do not know how similar physiological alterations shape recruitment of neuronal ensembles in the dmPFC that encode appetitive CS-US associations. Hence, we compared changes in excitability, synaptic physiology, and connectivity of behaviorally-activated neurons during the early stages (i.e. prior to the establishment of robust CS-evoked food seeking) and late stages of conditioning. Finally, we directly tested the importance of neuronal excitability changes in conditioned performance using a chemogenetic (DREADD) approach.

Materials and Methods

Animals:

Heterozygous (het) male *Fos-GFP* (RRID: IMSR_JAX:014135), *Fos-tTa* mice (RRID: MMRRC_031756-MU), *GAD-tdTomato* mice (Besser et al., 2015) (C57BL/6J-Tg(Gad2-tdTomato)DJhi; RRID:IMSR_EM:10422; were bred onto a C57BL/6 background. *TRE-H2B-GFP* (RRID:IMSR_JAX:005104) (Tumbar et al., 2004) mice previously bred onto a CD-1 background were bred with wild-type C57BI/6 females obtained from Charles River UK at the University of Sussex. het *TRE-H2B-GFP* mice were bred onto a C57BL/6 background for at least 6 generations before being bred with het *Fos-tTA* mice to generate double transgenic *TetTag H2B-GFP* mice. het Male *GAD-tdTomato* were bred with het *Fos-GFP* female mice to produce double transgenic *Fos-GFP x GAD-tdTomato* (*FGGT*) mice. The *Fos-GFP* het male mice used to characterize the time course of Fos-GFP expression (Fig. 2) were bred in a similar manner at the National Institute on Drug Abuse (NIDA) IRP (Bruce Hope lab, Baltimore, USA). *FGGT* male mice were used for 2-Photon imaging experiments (Experiment 1), *Fos-GFP* and *TetTag H2B-GFP* male mice were used for *ex vivo* electrophysiology experiments (Experiment 2). *Fos-tTa* and WT male mice were used for chemogenetics experiments (Experiment 3). All mice were housed under a 12-hours light/dark cycle (lights on at 7:00) at the maintained temperature of 21+/-1 °C and 50 +/-5% relative humidity. Mice used in the Fos-GFP expression time course experiment were ~20-25 weeks old at time of testing. For Experiments 1-3, mice were aged 7-13 weeks at the beginning of experimental procedures, and were food restricted (90% baseline body weight) 1 week prior to behavioral testing until the completion of behavioral experiments. The Fos-GFP expression time course experiment was carried out according to National Institutes of Health guidelines under experimental protocols that were approved by the Animal Care and Use Committee of NIDA IRP. Experiments 1-3 were conducted in accordance with the UK 1986 Animal Scientific Procedures Act (ASPA) and received approval from the University of Sussex Animal Welfare and Ethics Review Board.

Surgical Procedures:

Microprism implantation in FGGT mice (Experiment 1):

At ages 10-13 weeks, FGGT mice were implanted with a microprism in the mPFC. Microprism constructs were built by assembling 2 circular glass windows (5 mm and 3 mm diameter; #1 thickness, cat. no: 64-0700 and 64-0720, Warner instruments, Holliston, USA) and a 1.5 mm coated microprism (Model no: MPCH-1.5, part no: 4531-0023, Tower Optics, Boyton Beach, USA) using optical glue (Norland Optical Adhesive, Cranbury, USA), such that the microprism rested on the 3 mm window with its vertical imaging edge on the diameter. Mice were anesthetized with isoflurane 3% dilution in O_2 (0.8 L/min) and NO_2 (0.5 L/min) and maintained between 1 and 2% dilution throughout the surgery. They first received an injection of dexamethasone (Dexadreson, 5mg/kg, s.c. or i.m.) to reduce cerebral inflammation. The skin on their scalp was sectioned off and the skin around the section was glued to the skull (Vetbond, 3M, St. Paul, USA). The bone was then scored before a set of custom headbars was fixed to the skull using dental cement (Unifast TRAD, Tokyo, Japan). A 3 mm circular opening was created in the skull centered at bregma 0.8 mm (+/-0.2 mm according to the location of blood vessels).The final area observable through the microprism spanned approximately from bregma 0.05 mm to 1.55 mm on the rostro-caudal axis and from 0 mm to 1.5 mm on the dorso-ventral axis (of note, the most dorsal section was usually obscured by the central sinus). The vast majority of this area constitutes the anterior cingulate cortex of the mPFC (Fig.3A; Paxinos and Franklin, 2001). Microprism implantation occurred similarly as described in Low et al., (2014). The dura was removed and the microprism construct was lowered into the brain using a custom-built holder such that the microprism was positioned between the hemispheres with the imaging surface placed against the sagittal surface of one of the hemispheres (Fig. 3A). The construct was glued with Vetbond and further fixed with dental cement. Following implantation, mice received buprenorphine (0.1 µg/kg, i.m.) and were left to recover in a heated chamber for an hour. Following surgery, they received 3 days of oral Meloxicam (Metacam, Boehringer, Berks, UK). All mice recovered for a minimum of two weeks before undergoing any further procedures. The first imaging session typically occurred 3-4 weeks following surgery to allow inflammation in the imaging area to subside.

Generation of AAV particles

All AAV transgenes were packaged into AAV capsids, serotype AAV2. HEK293 cells were co-transfected with the transgene construct plasmid pAAV-PTRE-tight-hM3Dq-mCherry which was a gift from Prof. William Wisden (Zhang et al., 2015) (Addgene plasmid # 66795), the adenovirus helper plasmid pHelper (Stratagene) and the AAV2 helper plasmid pRC (Stratagene) using the calcium phosphate method. The cells were harvested and pelleted 72 hours after transfection and re-suspended in lysis buffer (150 mM NaCl, 20 mM Tris pH 8.0). Benzonase endonuclease (Merck; E1014) was added and the cell lysate was incubated at 37°C for 30 minutes, before being centrifuged and the supernatant purified by the iodixanol gradient method. Optiseal tubes (Beckman Coulter; 361625) were prepared with iodixanol gradients overlaid in the following order; 5 ml 15% in PBS-MK, 5 ml 25% in PBS-MK with phenol red, 6 ml 40% in PBS-MK, and 9 ml 60% with phenol red. The supernatant was then overlaid and the tube sealed, then centrifuged at 461000 g for 1 hour at 18°C. The AAV particles were collected from the 20% layer by piercing the tube horizontally with an 18G needle, and concentrated using Amico Ultra-4 (Merck; UFC810008) at 2000 g for a minimum of 20 minutes. The elution was re-suspended with 250 µl dPBS and aliquoted and stored at -80°C. The final titer was $1.67x10^{10}$ copies/ml.

Virus microinjection in mPFC of Fos-tTa and WT mice (Experiment 3):

7-12 week old *Fos-tTa* and WT mice received bilateral injections of AAV_2-TRE_{tight}-hM3Dq-mCherry (Zhang et al., 2015) in the medial prefrontal cortex (mPFC; coordinates: AP: bregma +1.2, ML +/- 0.5, DV – 1.2). Mice were anesthetized with isoflurane 3% dilution in O_2 (0.8 L/min) and NO_2 (0.5 L/min) and kept between 1 and 2% dilution throughout the surgery. Using a mounted drill, openings were created at the anterior-posterior and medio-lateral coordinates. Custom-built infusers – assembled from 26G 30 mm and 33G 65 mm stainless steel tubes (Coopers needle works LTD., Birmingham, UK) – were then lowered to the dorsal-ventral coordinates and 0.5 µL/hemisphere of virus was injected at a rate of 0.1 µL/min. The infusers remained in the brain 7 min before being raised gradually. Mice received Meloxicam (Metacam, Boehringer, Berks, UK) orally for 1 day prior to and 3 days post-surgery for analgesia and reducing inflammation. A week following surgery and

for the duration of the experiment, **all** mice received doxycycline in their drinking water (0.1 mg/mL) to prevent any unwanted transgene expression.

Behavioral experiments:

General Procedures (Experiment 1-3):

Similar behavioral experimental procedures and apparatus were utilized as in Ziminski et al., 2017. Briefly, behavioral experiments were performed in standard mouse operant chambers (15.9 x 14 x 12.7 cm; Med Associates, Vermont, USA), each fitted with a recessed magazine which dispensed 10% sucrose solution serving as the unconditioned stimulus (US) and a mechanical click generator providing a sound which served as a conditioned stimulus (CS). An infrared beam detected head entries into the food magazine. Mice were randomly assigned to 'Paired' or 'Unpaired' groups that underwent identical procedures except that Unpaired mice only received sucrose in the home cage 1-4 hours at random times before or after each conditioning (acquisition) session. As such, this group controlled for factors such as the effects of handling, chamber, CS and US exposure. One day following magazine training (in which Paired mice were pre-trained to the sucrose delivery magazine), mice underwent 12 acquisition sessions over a 7 day period for 1-2 sessions per day. Each 25 min acquisition session consisted of six 120s CS presentations, separated by 120s random –interval (RI) inter-trial interval periods. During each CS period 10% sucrose was delivered to the magazine (Paired mice) or was unrewarded (Unpaired mice) at a RI30 schedule. Twelve acquisition sessions produced selective responding to the CS.

Experiment-specific procedures:

Time course of Fos-GFP expression measured by GFP immunofluorescence: *Fos-GFP* mice in the 1.5, 8, and 18 hours condition were initially exposed to a novel context (plexiglass locomotor activity chamber, dimensions 43 (w) x 43 (l) x 30 (h) cm) for 25 min and then remained in their home cages for an additional 65 min, 7 hours 35 min, and 17 hours 35 min, respectively, and were subsequently deeply anesthetized and transcardially perfused with 4% paraformaldehyde. *Fos-GFP* mice in the 0 hour condition were transcardially perfused without being exposed to the novel context. GFP immunofluorescence was performed as described previously (Ziminski et al. 2017). Unless specified,

all steps were performed in room temperature. 30 µm sections containing the anterior cingulate cortex were prepared using a Leica CM1900 cryostat and sections were collected in Tris-buffered saline (TBS; 0.025 m Tris-HCl, 0.5 m NaCl, pH 7.5). Free-floating sections were washed in TBS and blocked in 10% normal goat serum (catalog #S-1000, RRID:AB_2336615; Vector Laboratories) in TBST (TBS, 0.2% Triton X-100). Next, slices were incubated at 4°C overnight in anti-GFP primary antibody (catalog #ab13970, RRID:AB_300798; Abcam) diluted 1/16000 in 3% normal goat serum TBST. The following day, slices were incubated for 2 hours in anti-chicken Alexa 488 (catalog # A-11039, RRID:AB_2534096, Thermo Fisher Scientific) at 1/200 in TBST. Slices were mounted on Superfrost Plus slides (catalog # 10149870; Thermo Scientific) air-dried, and coverslipped with PermaFluor (catalog #TA-030-FM, RRID: SCR_014787; Thermo Scientific).

Fluorescence images of Fos-GFP staining from left and right hemispheres of the dmPFC from two coronal sections per animal, corresponding to approximately bregma 0.7 and 1.2 (Paxinos and Franklin, 2001), were captured using a QI click camera (Qimaging) attached to an Olympus Bx53 microscope. GFP+ immunoreactive nuclei were quantified using iVision software (version 4.0.15, RRID: SCR_014786; Biovision Technologies). Layers II/III were selected for this analysis similar to our *in vivo* imaging and *ex vivo* electrophysiology experiments.

Experiment 1 (*in vivo* imaging): Acquisition sessions proceeded in Paired and Unpaired groups as described in *General Procedures* with a protruding feeding port to accommodate mice equipped with a head-restraint device. For acquisition sessions 1 (S1), 5 (S5) and 11 (S11), Unpaired mice received sucrose 10 minutes before training in their home cage, for all other sessions, sucrose was delivered at a random time during the day. 3 days following the last acquisition session, mice were tested for Pavlovian conditioning with a cue exposure test: both Paired and Unpaired mice were placed in the conditioning chamber and tested under extinction conditions for 3 CS presentations.

Experiment 2 (*ex vivo* electrophysiology): *Fos-GFP* mice were randomly assigned to S1 and S11 groups. Mice in the S1 group received only a single acquisition session (Paired or Unpaired as described in *General Procedures*) following magazine training before being sacrificed for

electrophysiology recordings. Unpaired mice received sucrose in their home cage 10 minutes before this session. Mice in the S11 group received 11 sessions of conditioning before being sacrificed for electrophysiology recordings. Unpaired mice received sucrose in their home cage 10 minutes before this session, for all other sessions it was delivered at a random time. *TetTag H2B-GFP* mice received only a single S1 acquisition session (Paired or Unpaired as described in *General Procedures*) following magazine training. Likewise, Unpaired mice received sucrose 10 minutes before the session. 3-7 d following this acquisition session, they were sacrificed for electrophysiology recordings.

Experiment 3 (chemogenetics): All mice were trained under Paired conditions and two main experiments 'S1 tag' and 'NC tag' were performed here. In both experiments, *Fos-tTA* and their negative, wild-type (WT) littermates (same genetic background) were injected with AAV_2-TRE_{tight}-hM3Dq-mCherry and underwent identical behavioral procedures except for the 'tagging session' which could either be a conditioning session as described in *General Procedures* ('S1 tag') or a 25 minute novel context exposure ('NC tag'). Previous studies have shown that novel context exposure recruits neurons that are unrelated to appetitive learning (Cruz et al., 2014), and thus this exposure served to tag such neurons here. Immediately following Magazine training, doxycycline was removed from the drinking water for 48 h at which point mice underwent the 'tagging session' to label activated neurons in *Fos-tTa* mice with hM3Dq. Importantly, hM3Dq expression persisted many days following the acquisition and recall sessions (Fig. 8B), indicating the reliability of our neuronal manipulation. An hour following this tagging session, mice received high doxycycline drinking water (1 mg/mL) for 24 hours before undergoing normal a conditioning session and receiving low doxycycline drinking water (0.1 mg/mL) for the remainder of the experiment. Conditioning sessions then proceeded as described in *General procedures* until the completion of a total of 12 conditioning sessions. Mice received injections of the hM3Dq agonist 'clozapine' (0.1 mg/kg, i.p. (Gomez et al., 2017) 15 minutes prior to the beginning of every two sessions (Fig. 8A). This compound is a metabolite of the widely-used hM3Dq agonist clozapine-*N*-oxide (CNO), clozapine has recently been shown to serve as the agonist at hM3Dq (Gomez et al., 2017). Thus, clozapine compared to CNO has a direct mode of action at hM3Dq and does not depend on metabolic function. To habituate mice to injections, 4-5

saline injections were delivered to them over the week preceding training. Three days following the last acquisition session, mice were tested for Pavlovian conditioning with a cue exposure test: Paired mice were placed in the conditioning chamber and tested under extinction conditions for 6 CS presentations.

Electrophysiology (Experiment 2)

Brain slice preparation:

Ninety min following S1 or S11 (*Fos-GFP* mice) and 3-7 d following S1 (*TetTag H2B-GFP* mice), mice were deeply anaesthetized with ketamine and xylazine and transcardially perfused with ice cold NMDG-HEPES recovery aCSF (in mM, 93 NMDG, 2.5 KCl, 1.2 NaH_2PO_4, 30 $NaHCO_3$, 20 HEPES, 25 glucose, 2 thiourea, 5 Na-ascorbate, 3 Na-pyruvate, 0.5 $CaCl_2 \cdot 4H_2O$ and 10 $MgSO_4 \cdot 7H_2O$, bubbled with 95% O_2/ 5% CO_2, pH 7.4, 305-310 mOsm/kg)(Ting et al., 2014). The brain was quickly removed and sliced in NMDG-HEPES aCSF on a Leica VT1200S vibratome to 250 µm thick sections between bregma 1.70 to 0.86 mm containing the mPFC. Sections were incubated in 34ºC NMDG-HEPES aCSF for 5 min and transferred to standard recording aCSF (in mM, 126 NaCl, 4.5 KCl, 1 $MgCl_2$, 2.5 $CaCl_2$, 1.2 NaH_2PO_4 11 D-(+)-Glucose, 26 $NaHCO_3$ bubbled with 95% O_2/5% CO_2, pH 7.4) at room temperature for the remainder of the recording day. Slices were transferred to a recording chamber perfused with 30-32ºC standard aCSF at 2-3 ml/min. Neurons were visualized with differential interference contrast using an Olympus BX51WI microscope attached to a Revolution XD spinning disk confocal system (Andor 252 Technology Ltd) for fluorescence microscopy.

GFP+ neurons were identified with a 488 nm excitation wavelength; neurons which did not express visible GFP were considered to be GFP negative (GFP–). Whole-cell recordings on layer II-III mPFC pyramidal neurons were performed using borosilicate capillary glass-pipettes (1.5 mm outer diameter, 0.86 mm inner diameter), for intrinsic excitability and connectivity recordings filled with (in mM): 135 K-gluconate, 3 MgCl2, 4 NaCl, 5 HEPES, 5 EGTA, 2 Mg-ATP, 0.3 Na3-GTP (pH 7.25) and 100 µM Alexa 568 dye (A10437, ThermoFisher Scientific). For synaptic recordings (in mM): 0.1 Spermine, 120 CsCH3SO3, 5 NaCl, 10 TEA-Cl, 10 HEPES, 1.1 EGTA, 4 MgATP, 0.3 Na-GTP, 0.001

QX314 (Lidocaine, Sigma-Aldrich) and 1% biocytin (Sigma-Aldrich). Pipette resistances ranged from 4-7 MΩ. Neurons were confirmed to be GFP+ during recording by co-localization of GFP and Alexa 568. Pyramidal neurons were identified based on their morphology and/or characteristic firing properties (Cao et al., 2009). Data were collected with a Multiclamp 700B amplifier (Molecular Devices), A/D board (PCI 6024E, National Instruments) and WinWCP and WinEDR Software (courtesy of Dr. John Dempster, University of Strathclyde, Glasgow, UK; http://spider.science.strath.ac.uk/sipbs/software_ses.htm). Signals were amplified, filtered at 4 kHz and digitized at 10 kHz. The Hum Bug noise eliminator (Quest Scientific) was used to reduce noise.

Intrinsic excitability recordings:

Pyramidal neurons were held at -65 mV for the duration of recording. The current clamp protocol consisted of 800 ms positive current injections from -60 pA incrementing in 4 pA steps. The liquid junction potential was -13.7 mV and was not accounted for. Spike counts were conducted using Stimfit (Guzman et al., 2014) while spike kinetics were analyzed with MiniAnalysis software (MiniAnalysis, Synaptosoft). See Table 1 for details on spike kinetic analysis.

Synaptic physiology recordings:

Recordings were undertaken in the presence of the GABAA channel blocker picrotoxin (100 μM; Sigma-Aldridge). sEPSCs were analyzed over a 30 s period with MiniAnalysis. Responses were evoked using 0.1 ms pulses through bipolar theta glass pipettes filled with extracellular solution, within 200 μm of the neuron. Series resistance was monitored using -10 mV voltage steps (100 ms) and only cells maintaining stable access (<15% change) were included in the analyses. Paired-pulse ratios (PPR) were calculated by stimulating twice in succession and dividing second peak by the first peak (average of triplicate), across inter-stimulation intervals of 20, 40, 60, 80, 100, 150 and 200 milliseconds. AMPAR/NMDAR current ratios were calculated from the averages of 10-20 evoked EPSCs at +40 mV with and without D-APV (50 μM, Cat #: HB0225, Hello Bio). For each neuron, the AMPAR current (with D-APV) was subtracted from the combined current (without D-APV) to yield the NMDAR current. AMPAR current peak was divided by NMDAR current peak to yield AMPAR/NMDAR ratios. Traces in figures have stimulus artefacts removed.

Connectivity Recordings:

Pairs of pyramidal neurons located within 60 µm were targeted for dual recordings. Single action potentials were elicited from 'Presynaptic' neurons in current clamp mode using a 5 ms step current. 'Postsynaptic' neurons held in voltage clamp mode at -70 mV. A 'connection' was deemed if a presynaptic AP elicited an excitatory postsynaptic current response in at least 50% of 50 sweeps. Upon completion of recording, assessment of connectivity was conducted in the opposite direction.

Histology (Experiment 3):

Fos-tTa and WT mice were anesthetized with 200 mg/kg, i.p. sodium pentobarbital and transcardially perfused with 4% paraformaldehyde (PFA). To assess mCherry expression, free-floating sections were washed in Tris-buffered saline (TBS: 0.025 M Tris-HCl, 0.5 M NaCl, pH 7.5) and blocked in 10% normal goat serum (Cat # S-1000, VectorLabs, RRID:AB_2336615) in TBST (TBS, 0.2% Triton-X 100). Slices were incubated at 4 °C overnight in anti-mCherry primary antibody (Cat # ab205402, Abcam, RRID: AB_2722769) diluted 1/2000 In 3% normal goat serum TBST. The following day slices were incubated 2 h in anti-chicken 568 antibody (Cat# 20104-1, Biotium, RRID: AB_10853460) at 1/200 in TBST. Slices were mounted on Superfrost Plus slides (Cat # UY-48512-00, Cole-Parmer), air-dried, and coverslipped with PermaFluor (Cat#TA-030-FM, Thermo Scientific, RRID: SCR_014787). Fluorescence images of mCherry staining (Fig. 7B) from both left and right hemispheres of the anterior cingulate cortex of 2-4 coronal sections per animal, corresponding approximately to Bregma 1.2 (Paxinos and Franklin, 2001), were captured using QI click camera (Qimaging) attached to an Olympus Bx53 microscope (Olympus). *Fos-tTA mice* not expressing mCherry (n=2) were excluded from the study.

***in vivo* 2-Photon imaging (Experiment 1):**

Habituation and imaging sessions:

Imaging sessions took place on head-fixed, awake mice that were able to freely run on a polystyrene cylinder (Fig. 3C). For ~1 week prior to the first imaging session, mice were habituated to being restrained by being head-fixed regularly for progressively increasing durations. Following habituation, the brain surface under the microprism was assessed and 2 to 3 areas of interest were defined. In

each area of interest, z-stacks in both the red and green channels were recorded simultaneously at an excitation wavelength of 970 nm (power at the objective: 70-130 mW; pixel dwell time: ~3.9 ns) from the pial surface to a depth of approximately 300 µm. Each slice of the stack was an average of two 660.14 x 660.14 µm images (corresponding to 512 x 512 pixels; pixel size: 1.2695 x 1.2695 µm). Images were captured in pre-defined areas of interest using a Scientifica multiphoton microscope (Uckfield, UK) with a 16X water immersion objective (CFI LWD Plan Fluorite Physiology objective, NA 0.8, WD 3mm; Nikon Corporation, Tokyo, Japan) and a Chameleon Vision-S Ti:Sapphire laser with dispersion precompensation (Chameleon, Coherent, Santa Clara, USA). The software used for recording was ScanImage r3.8 (Pologruto et al., 2003).

Imaging sessions took place 75 min following initiation of the 1st, 5th and 11th conditioning session as well as the cue exposure test (Fig. 3C). Another two imaging sessions took place directly from the home cage (2-3 days prior to conditioning and 5-8 days after the cue exposure test). Imaging sessions typically lasted 40 minutes to an hour. Of note, GFP expression observed during imaging is unlikely to be caused by previous behavioral sessions as imaging took place exclusively following AM sessions, approximately 18 hours from the previous PM session where GFP expression returns to baseline levels (Fig. 2A). Due to poor imaging quality on one or several imaging sessions, three mice (1 unpaired, 2 paired) were excluded from image analysis.

Analysis:

Image Analysis:

Initial image processing took place in FIJI (ImageJ; Schindelin et al., 2012). tdTomato images within a stack were aligned to each other on x and y axes with MultiStackReg (Thevenaz et al., 1998). The resulting transformation was then applied to the GFP image stack. Stacks were aligned between sessions using the Landmark Correspondence plugin (Stephen Saalfeld). An overlapping volume within layer II/III and common to all sessions was identified and selected. All images in the selected stacks were despeckled and an FFT bandpass filter (upper threshold 40 pixels, lower threshold 5 pixels) was applied. Local maxima (noise tolerance: 30 pixels) were identified and the signal within a disk around the maxima (12 pixel diameter (15.234 µm) for GFP ‘signal’ and 16 pixels diameter

(20.312 µm) for tdTomato signal) was compared to the 'noise' surrounding it (2.5390 µm thick band, 1.2695 µm away from the disk). A cell was considered GFP+ or tdTomato+ (as appropriate) if 'signal' > 'noise' + 2.3 SD (noise) for at least two consecutive slices in the stack (Fig. 3B). Positive cells were recorded in an empty 3D matrix the size of the stack and later the x, y, z coordinates of each cell were extracted from the matrix using 3D object counter (Bolte and Cordelières, 2006).

A custom Matlab (2016a, MathWorks, Natick USA) script defined whether each cell was a putative 'interneuron' or 'pyramidal cell' according to whether tdTomato signal was detected in a cell for a majority of recorded sessions. Repeatedly activated neurons were then identified by sorting cells according to their expression in all recording sessions. For each session, a cell's x, y, z coordinates were compared to those obtained from previous sessions. If the x, y and z coordinates fell within a 20 pixel interval (25.390 µm) of existing coordinates, it would be considered the same cell. If several existing coordinates fulfilled this condition, the cell was assigned to the closest set of coordinates on the x, y plane as defined by Euclidean distance. If no coordinates fulfilled this condition, the cell was considered newly activated. To account for inter-individual difference in cell density, GFP expression as well as any possible damages cause by microprism implantation to the tissue, all variables relating to GFP+ quantification were normalized to the average number of GFP+ cells detected in home cage sessions which was considered our baseline activation level (Fig. 3D).

Experimental Design and Statistical Analysis:

In the main text, we report all main and interaction effects that are key to data interpretation. All data were analyzed using GraphPad Prism (RRID:SCR_002798; GraphPad Software) and SPSS (IBM SPSS Statistics, Version 23.0 (2015), Armonk, NY: IBM Corp). Group data are presented as mean±SEM.

Fos-GFP time course expression data: All sample sizes are detailed in the legend of Figure 2. The goal of this experiment was to measure the number of activated neurons GFP-expressing in the dmPFC at different time points following novel context exposure (Fig. 2A). To this end, *Fos-GFP* mice were randomly assigned the 0, 1.5, 8, and 18 hours groups. Thus, depending on condition,

Fos-GFP mice in the 1.5, 8, and 18 hours condition were initially exposed to a novel context for 25 min and then remained in their home cages for an additional 65 min, 7 hours 35 min, and 17 hours 35 min, respectively, and subsequently were deeply anesthetized and transcardially perfused with 4% paraformaldehyde. *Fos-GFP* mice in the 0 hour condition were transcardially perfused without being exposed to the novel context. Following perfusions, we removed their brains and processed them for Fos-GFP immunohistochemistry. GFP expression data were analyzed using a one-way ANOVA in Prism, followed by post-hoc testing (Sidak correction).

Experiment 1: Behavior and *in vivo* 2P imaging. All sample sizes are detailed in the legends of Figures 1, 3, and 4. The broad aim of this experiment was to characterize Fos-GFP expression patterns in activated pyramidal cells (Fos-GFP+/tdTomato– cells) and interneurons (Fos-GFP+/tdTomato+ cells) as a function of appetitive conditioning and memory recall (Figs. 3 and 4). To this end, FGGT mice were randomly divided into Paired (conditioned) and Unpaired (control) groups, then underwent behavioral training (Fig. 1) and 2P imaging following S1, S5, and S11 of conditioning and a test for Recall (Figs. 3C and 4).

First, to determine if Paired FGGT mice acquired a CS-US association, we measured head entries into the sucrose delivery magazine during the CS (cue-on) and ITI (no cue) periods (Figs. 1A and 1B). This data was analyzed using a three-way mixed ANOVA using the factors of Cue (cue-on, no cue), Session, and Group (Paired, Unpaired; Fig. 1B). Additionally, for the Paired group only, we calculated selectivity indices (CS entries – ITI entries) / Total entries) and analyzed them using one-way repeated measures ANOVA in SPSS (Figs. 1D). A proportion of mice from these groups were randomly selected to undergo cue-evoked food seeking in Recall (Fig. 1C). These data were analyzed using a two-way mixed ANOVA in Prism using the factors of Cue and Group. Following the two-way mixed ANOVA, a further post-hoc test was performed (Sidak correction) since an interaction was observed ($P<0.05$).

We performed 2P imaging of GFP+ pyramidal cells and interneurons during baseline, conditioning and Recall. Pyramidal cells and interneurons are affected differently by glutamatergic signaling

(Riebe et al., 2016) suggesting distinct Fos induction thresholds, as such they were analyzed separately. Due to poor imaging quality on one or several imaging sessions, three mice (1 Unpaired, 2 Paired) were excluded from image analysis. In order to determine if baseline GFP+ counts for pyramidal cells and interneurons were similar between groups, we examined the number of GFP+ neurons per mm^3 with a two-way mixed ANOVA using the factors of Group and Session in Prism (Fig. 3D). Subsequent GFP+ counts were normalized to this baseline. To examine if the number of GFP+ neurons were modulated as a function of conditioning, we performed two-way mixed ANOVAs using the factors of Group x Session in Prism (Fig. 4A). We also examined whether conditioning modulated the number of repeatedly activated neurons according to their S1 activation history (S1+| S5+ S11+, S1- S5+ S11+), and performed two-way mixed ANOVAs using the factors of Activation History and Group in Prism (Fig. 4C). Following two-way mixed ANOVAs, further post-hoc tests were performed (Sidak correction) if an interaction was observed ($P<0.05$). The results from the Recall test were analyzed for differences in Fos-GFP+ neurons using t tests in Prism (Fig. 4E). Additionally, to determine whether conditioning modulated the number of recall-activated GFP+ neurons with a repeated activation history during conditioning according to their S1 activation (S1+| S5+ S11+ R+ or S1-| S5+ S11+ R+), we performed two-way mixed ANOVAs using the factors of Activation history and Group (Fig. 4F). Further post-hoc tests were performed (Sidak correction) if an interaction was observed ($P<0.05$). Also, to better characterize the proportion of neurons recruited in S1 and Recall according to their subsequent (Fig. 4D) and previous reactivation patterns (Figs. 4G), as well as characterizing the reactivation of repeatedly activated neurons (S1+| S5+ S11+) in Recall (Fig. 4H), chi-squared tests were performed on pooled neurons (Activation history X Group) in SPSS and further post-hoc procedures (Beasley and Schumacker, 1995); Bonferroni correction) performed if a significant interaction was observed ($P<0.05$).

Experiment 2: *Ex vivo* electrophysiology. All sample sizes are detailed in the legends of Figures 5, 6 and 7. The purpose of the electrophysiological experiments was to reveal the intrinsic, synaptic and connectivity properties of recently activated GFP+ neurons and their surrounding GFP– neurons following the early (S1) and late (S11) phases of conditioning. Similar to Experiment 1, *Fos-GFP* and *TetTag H2B-GFP* mice were randomly assigned into Paired (conditioned) and Unpaired (control)

groups and underwent identical behavioral training procedures. 1.5 hours following training session onset at S1 or S11 (*Fos-GFP* mice) and 3-7 d following S1 (*TetTag H2B-GFP* mice) their brains were removed for electrophysiological analyses. Spike counts (Fig. 5A-C) were analyzed separately at S1 and S11 (unless specified otherwise in text), using three-way mixed ANOVAs including the factors of Group, GFP (GFP+, GFP–) and a repeated measures factor of Current (12 pA increments) in SPSS. Other intrinsic active and passive membrane properties (Tables 1 and 2) and synaptic properties (AMPAR/NMAR ratio, sEPSC amplitude and frequency; Fig. 6A-C) were analyzed using two-way ANOVAs with Group and GFP as factors, with S1 and S11 analyzed separately in Prism. Paired pulse ratios were analyzed using a three-way mixed ANOVA including the factors of Group, GFP, and inter-stimulus interval (ISI, in ms: 20, 40, 60, 80, 100, 150, 200) in SPSS (Fig. 6D). Connectivity (Fig. 7) was determined using Fischer's Exact test on 2 X 2 frequency matrices (column: Paired, Unpaired; row: Connected, Unconnected) separately for each pair type (+/+, +/–. –/+) and session condition (S1, S11) in SPSS. Average connectivity was calculated as: (sum of all connected pairs / total connections tested)*100. Outliers were detected using GRUBBS detection test ($\alpha = 0.05$) in Prism and excluded from analyses. Post-hoc tests were conducted using a Sidak's multiple comparisons test, if significant interactions were observed.

Experiment 3: DREADD manipulation of S1- and NC-tagged neurons. All sample sizes are detailed in the legends of Figure 8. The goal of this experiment was to examine the behavioral effects of chemogenetically, repeatedly increasing the excitability of S1-tagged (activated) neurons on appetitive conditioning. The experimental timeline is shown in Fig. 8A. To this end, Fos-tTa mice and their negative, wild-type (WT) littermates were injected with AAV_2-TRE_{tight}-hM3Dq-mCherry in the dmPFC for two separate experiments, 'S1 tag' and novel context or 'NC tag' (to rule out effects of general tagging). Fos-tTA and WT mice were randomly assigned to the S1 and NC tag conditions. Data from these conditions were analyzed separately.

In order to determine if repeated hM3Dq activation of S1- and NC-tagged neurons via clozapine modulated conditioning, head entries (Figs. 8D and 8G) were analyzed using three-way mixed ANOVAs using the factors of Genotype (Fos-tTA, WT), Cue, and Session in SPSS, and the

selectivity index data (Figs. 8C and 8F) were analyzed using two-way mixed ANOVAs using the factors of Genotype and Session in Prism. Following two-way mixed ANOVAs, further post-hoc tests were performed (Sidak correction) if an interaction was observed ($P<0.05$). To test the effects of repeated hM3Dq activation on cue-evoked food-seeking during Recall, head entries were analyzed using two-way mixed ANOVAs using the factors of Genotype and Cue in Prism (Figs. 8E and 8H).

Results

Appetitive conditioning shapes CS-selective approach behaviors in *FGGT* mice

Microprism-implanted *Fos-GFP x GAD-tdTomato (FGGT)* mice were trained on a simple appetitive conditioning task (Fig 1A) under freely-moving conditions. Across the 12 acquisition sessions (1-2 sessions per day), mice assigned to the Paired group received repeated trials during which an auditory cue (CS) was paired with liquid sucrose delivery (US). Mice in the Unpaired (control) group received an equal number of CS presentations in the conditioning chamber, but received sucrose in their home cage only. As such, this group controlled for factors such as the effects of handling, and exposure to the conditioning chamber, CS and US. Three days following the last acquisition session, mice were tested on a CS-US memory recall test conducted under extinction conditions (Fig. 1A). Similar to our recent study (Ziminski et al., 2017), initial analysis of acquisition and recall test performance revealed significant interaction effects of Cue X Session X Group (Fig. 1B; $F_{11,220}$=5.94, P<0.001) and Group X Cue (Fig. 1C; $F_{1,11}$=15.46, P<0.01), respectively, indicating cue-selective approach responding or food seeking during the CS versus the Inter-Trial Interval (ITI, no cue) periods. We further assessed conditioning performance by calculating a 'Selectivity Index' (Fig. 1D) by subtracting ITI from CS-trial head entry counts and normalizing to total head entries. During acquisition, there was a significant effect of Session ($F_{11,121}$=9.50, P<0.001) in the Paired group, indicating that Paired mice came to selectively respond to the CS as a function of training.

The time course of Fos-GFP expression

In *Fos-GFP* mice, a transgene containing a *c-fos* promoter drives expression of a gene encoding a fusion protein of Fos and green fluorescent protein (GFP) in behaviorally-activated neurons (Barth et al., 2004; Koya et al., 2012). We characterized the time course of GFP expression in the dorsal mPFC (dmPFC) following 0, 1.5, 8, and 18 hours exposure to a novel context (locomotor activity chamber). A one-way ANOVA followed by post-hoc testing revealed that GFP expression was significantly elevated at 1.5 compared to 0, 8, and 18 hours and that there were no differences between the 0, 8, and 18 hours groups. ($F_{3,15}$=19.72, P<0.001; Fig. 2A). Thus, GFP expression peaked at 1.5 hours and returned to baseline levels at 8 and 18 h. These and other findings (Barth

et al., 2004; Cifani et al., 2012) further validate the use of Fos-GFP as a recent, but not a remote marker, of neuronal activity. Hence, we performed our *in vivo* imaging and *ex vivo* electrophysiological characterization of Fos-GFP-expressing neurons following ~1.5 hours from the initiation of behavioral testing.

As the CS-US association is established, a stable neuronal ensemble is recruited from a wider pool of neurons activated in the initial conditioning session

We used 2P imaging in microprism-implanted *FGGT* mice to characterize activation among pyramidal cells (tdTomato–) and interneurons (tdTomato+) in layers II/III of the dorsal medial prefrontal cortex (dmPFC; Fig. 3A, B, C). In order to assess baseline GFP expression, we first examined the number of GFP+ pyramidal cells and interneurons per mm^3 in mice that have been in the home cage (HC) for at least 24 h. Imaging sessions were conducted both before (HC1) and after (HC2) mice underwent behavioral training. We observed no significant interaction effect of Group X Session for pyramidal cells ($F_{1,17}$=0.02, P=0.89) and interneurons ($F_{1,17}$=1.84, P=0.19; Fig. 3D). Thus, behavioral training did not modulate baseline GFP expression for both cell types. In further analyses, to account for inter-individual differences in cellular density and GFP expression, the number of HC1 and HC2 GFP+ pyramidal cells and interneurons were averaged for each mouse and used to normalize subsequent GFP+ cell counts.

Approximately 80-90 min following the initiation of the 1st, 5th, and 11th acquisition sessions and the recall session, we used 2P imaging to characterize neuronal activation patterns among pyramidal cells and interneurons in the dmPFC (Fig. 3A, B, C). Hence, the observed GFP expression reflects neuronal activity of the dmPFC during the behavioral sessions under freely moving conditions. We first assessed the overall number of strongly activated, GFP+ pyramidal cells and tdTomato+ interneurons on the 1st (S1), 5th (S5), and 11th (S11) conditioning sessions (Fig 4A), which occurred 2-3 days apart from each other (since 1-2 sessions are conducted per day). No significant interactions of Group X Session were observed in pyramidal cells ($F_{2,34}$=0.20, P=0.82) or interneurons ($F_{2,34}$=0.06, P=0.95), indicating that the total number of activated neurons across acquisition sessions did not fluctuate as a function of conditioning for either cell type in the dmPFC.

Repeated, persistent activation of the same set of neurons in the nucleus accumbens underlies conditioning using a drug reward, suggesting that such neurons with repeated activation history encode associative information (Mattson et al., 2008). Moreover, activity in the motor cortex early in learning of a simple motor task is a critical determinant for ensemble consolidation (Cao et al., 2015). Thus, we investigated whether appetitive Pavlovian conditioning preferentially recruits a learning-relevant, repeatedly activated ensemble from a wider pool of candidate neurons activated at S1, prior to the development of a robust CS-evoked food seeking response. To this end, Unpaired and Paired groups were assessed and compared for the number of GFP+ neurons in two distinct 'Activation History' categories: neurons that were persistently activated (+) in S5 and S11, following activation in S1 (S1+| S5+ S11+), or neurons activated in S5 and S11, but that were not activated on the initial conditioning session (S1-| S5+ S11+; Fig. 4B & 4C). In pyramidal cells, there was a significant interaction effect of Activation History X Group ($F_{1,17}$=5.97, P<0.05), followed by a significant main effect of Activation History ($F_{1,17}$=61.75, P<0.001), but not Group ($F_{1,17}$=1.17, P=0.29). Conversely, there was no significant interaction effect of Activation History X Group in interneurons ($F_{1,17}$=0.17, P=0.68), but a significant main effect of Activation History ($F_{1,17}$=8.10, P<0.05), but not Group ($F_{1,17}$=1.10, P=0.31). Hence, conditioning recruited a repeatedly activated ensemble from a pool of pyramidal cells activated in S1.

Having established the relevance of S1 activation to the development of a neuronal ensemble as a function of conditioning, we wanted to better characterize neurons recruited in S1 and in particular, their subsequent reactivation patterns (Fig. 4D). To this end, we assessed the proportion of S1-activated neurons that were reactivated in S5 only (S1+| S5+ S11-), S11 only (S1+| S5- S11+) or S5 and S11 (S1+| S5+ S11+) as well as neurons activated in S1 but not S5 and S11 (S1+| S5- S11-). During conditioning, there was a significant interaction of Activation History X Group for both pyramidal cells (X^2_3=58.98, P<0.001) and interneurons (X^2_3=41.63, P<0.001). Of note, there was a significantly higher proportion of S1+| S5+ S11+ neurons reactivating in Paired mice compared to Unpaired mice (P<0.05) for both pyramidal cells and interneurons. Furthermore, only 29% of S1-activated neurons were recruited into the persistently activated ensemble (S1+| S5+ S11+).

We also characterized neuronal activation patterns of pyramidal cells and interneurons following the Recall test (Fig. 4E). We observed a significantly higher number of pyramidal cells recruited following Recall in Paired mice compared to Unpaired mice (t_{10}=2.40, P<0.05). We did not observe a significant effect in interneurons (t_{10}= 0.67, P=0.52).

Next, we compared the number of GFP+ neurons activated during the test for recall with a S1+| S5+ S11+ or S1-| S5+ S11+ activation history (Fig. 4F). In pyramidal cells, there was a significant interaction effect of Activation History X Group ($F_{1,10}$=7.65, P<0.05), and main effects of Activation History ($F_{1,10}$=155.3, P<0.001) and Group ($F_{1,10}$=5.90, P<0.05). Post-hoc testing revealed a significant increase in the number of S1+| S5+ S11+ neurons activated during Recall (S1+| S5+ S11+ R+) in Paired mice compared to Unpaired mice (P<0.01). There was no significant interaction of Activation History X Group in interneurons ($F_{1,10}$=0.24, P=0.64), but a significant main effect of Activation History ($F_{1,10}$=44.69, P<0.001), but not Group ($F_{1,10}$=1.93, P=0.20). Thus, similar to the conditioning phase, memory recall recruited an ensemble that was persistently activated from a pool of pyramidal cells activated in S1.

We also assessed the proportion of Recall-activated neurons that had been repeatedly reactivated in Acquisition following activation in S1 ((S1+| S5+ S11-), (S1+| S5+ S11+), (S1+| S5- S11+); Fig.4G). There was a significant interaction of Activation History X Group for both pyramidal cells (X^2_3= 77.51; P<0.001) and interneurons (X^2_3= 13.54; P<0.001). Notably, there was a significantly higher proportion of Recall-activated pyramidal cells and interneurons also activated in Acquisition S1, S5 and S11 in Paired mice compared to Unpaired mice (P<0.05). There was also a higher proportion of pyramidal cells with a S1+| S5+ S11- history, suggesting S1 recruitment may be involved in conditioning-specific activation dynamics beyond the recruitment of a stable ensemble. Furthermore, only 23% of Recall-activated pyramidal cells exhibited a repeated activation history during conditioning (S1+| S5+ S11+).

Of note, 65% (UP) to 66% (P) of pyramidal cells and 61% (UP) to 63% (P) of interneurons that were repeatedly activated in acquisition (S1+|S5+ S11+) were reactivated in Recall (Fig. 4H). There was

no significant interaction of Group X Activation history for pyramidal cells (X^2_1= 0.42, P=0.52) or interneurons (X^2_1= 0.55, P=0.46), suggesting that conditioning does not modulate the likelihood of reactivation of persistently activated neurons in Recall. A point to consider here is that while a similar proportion of persistently activated neurons are reactivated in Recall in both groups, this reflects a greater number of these persistently activated neurons in the Paired group compared to the Unpaired group following conditioning. This is a result of persistently activated neurons being more numerous in Paired mice.

Taken together, we demonstrate that during the establishment and recall of a CS-US association, a stable, persistently activated ensemble is recruited in the mPFC from a pool of pyramidal cells that were initially activated in S1, when the acquisition of robust CS-US representations is yet to occur. Thus, activation in early learning may be a factor in allocating neurons to a stable conditioning specific ensemble.

Activation of a hyper-excitable pool of neurons following the initial conditioning session

Having established activation at S1 as a potential factor that modulates recruitment of neurons into an ensemble, we next determined the physiological properties of pyramidal cells activated during the initial conditioning session, prior to the development of cue-selective food seeking. The regulation of GFP+/GFP– excitability is thought to improve the signal-to-noise ratio of activated ensemble neurons (Whitaker and Hope, 2018). Thus, we initially analyzed the excitability of GFP+ and GFP– pyramidal cells in Paired and Unpaired *Fos-GFP* mice 90 min following initiation of S1 and observed significant alterations in firing capacity across groups (Fig. 5A; Group X Cell Type X Current $F_{12,600}$=6.38, P<0.001). Further analysis revealed a significant difference in excitability between GFP+ and GFP– neurons in Paired (Cell Type X Current, $F_{12,348}$=9.42, P<0.001), but not Unpaired mice (Fig. 5A; $F_{12,252}$=0.69, P=0.76). We then examined the underlying intrinsic adaptations that may contribute to the increased firing capacity of GFP+ neurons (Table 1). In Paired mice only, the input resistance (Ri) as measured by shifts in the current-voltage (I/V) curves of GFP+ neurons increased following S1 (Group X Cell Type X Current, $F_{25,1200}$=3.81, P<0.001; Paired: Cell Type X Current, $F_{25,700}$=6.85, P<0.001). Similarly, we observed a decrease in the rheobase or current necessary to

elicit an action potential (Group x Cell Type, $F_{1,49}$=6.64, P<0.05). We observed no other interaction effects for the action potential peak, half width, threshold, or afterhyperpolarization (AHP; both fast and medium). Taken together, S1 activated a pool of GFP+ neurons that were hyper-excitable compared to GFP– neurons. This hyper-excitability is associated with conditioning as it was not observed in GFP+ neurons of control mice that received unpaired presentation of sucrose and the cue.

Next, we determined whether the hyper-excitability of neurons activated on S1 persisted across days following acquisition (Fig. 5C). To address this question, we tagged neurons activated following S1 in Paired and Unpaired *TetTag H2B-GFP* mice (Tayler et al., 2013) and measured their intrinsic excitability 3-7 d following training under baseline conditions.

We observed no selective alterations in firing capacity (Group X Cell Type X Current, $F_{12,588}$=1.77, P=0.97) nor any significant interactions of Group X Cell Type for all other intrinsic properties (Table 2). We did observe a main effect of Cell Type in the firing capacity ($F_{12,588}$=3.62, P<0.001) associated with an increase in the I/V curves of H2B-GFP+ neurons ($F_{25,1225}$=5.01, P<0.001), indicating behaviorally-activated dmPFC neurons generally exhibit a mild increased baseline excitability (Fig. 5C; Table 2). Thus, although we did not examine excitability properties related to acute behavioral arousal immediately following S1 in TetTag H2B-GFP mice, taken together with the Fos-GFP mice findings from S1 suggests that the hyper-excitability of the S1-activated neuronal pool is not persistently maintained.

We next determined the excitability properties of neurons activated in late conditioning following S11. We analyzed the excitability of GFP+ and GFP– pyramidal cells following S11. We observed no alterations in firing capacity across groups (Fig. 5B; Group X Cell Type X Current, $F_{12,744}$=1.21, P=0.27). We did observe a significant interaction effect in the I/V curves (Group X Cell Type X Current, $F_{25,1550}$=2.16, P<0.001), underpinned by a GFP– increase in Unpaired mice (Cell Type X Current, $F_{25,700}$=2.93, P<0.001) and a significant fAHP interaction (Group X Cell Type, $F_{1,61}$=4.73, P<0.05) driven by a GFP– decrease in Paired (P<0.05) but not Unpaired (P=0.50) mice, suggesting

that some modulation of underlying parameters did occur (Table 1). We detected no other interaction effects in any other measured electrophysiological properties.

To confirm that the hyper-excitability of activated neurons we had observed in S1 was transient, we directly compared the firing capacity of GFP+ and GFP– neurons across S1 and S11 in Paired mice. As expected, we observed a significant change in firing capacity between S1 and S11 (Session X Cell Type X Current, $F_{12,756}$=4.38, P<0.001). This was driven by an increase in the excitability of GFP+ neurons in S1 compared to S11 ($F_{12,384}$=2.70, P<0.01) concurrent with a decrease in the excitability of GFP– neurons ($F_{12,372}$=1.81, P<0.05). Underpinning this alteration was a shift in the I/V curves of Paired mice (Figs. 5A and B (inset); Session X Cell Type X Current, $F_{25,1550}$=5.02, P<0.001), due to an increase in GFP+ neurons ($F_{25,800}$=3.34, P<0.001) and a decrease in GFP– neurons ($F_{25,750}$=1.89, P<0.01). We also observed a significant change in the medium afterhyperpolarisation (mAHP; Session X Cell Type $F_{1,62}$=10.50, P<0.01) determined by an increase in GFP– neurons (P<0.05) but not GFP+ neurons at S1.

In the Unpaired group, we observed no significant changes in firing capacity of GFP+ and GFP– neurons between S1 and S11 (Group X Cell Type X Current, $F_{12,588}$=0.88, P=0.57). We did observe an interaction effect on S1 and S11 I/V curves (Figs. 5A, B (inset); Session X Cell Type X Current $F_{25,1200}$=1.54, P<0.05), underpinned by an increase in GFP– ($F_{25,575}$=3.13, P<0.001) but not GFP+ ($F_{25,625}$=0.45, P=0.99) neurons and in the rheobase ($F_{1,62}$=4.79, P<0.05). Together, our findings reveal how hyper-excitability in behaviorally-activated neurons occur via bidirectional modulation of excitability in activated and non-activated neurons.

Conditioning-selective synaptic alterations are not observed in neurons activated in S1 and S11

Alterations in synaptic strength are thought to encode associative memories (Takeuchi et al., 2014). We therefore examined glutamatergic pre- and post-synaptic function in GFP+ and GFP– neurons following S1 and S11. We assessed synaptic strength using the AMPAR/NMDAR ratio, spontaneous excitatory post-synaptic current (sEPSC), and presynaptic release properties using paired-pulse ratios (PPRs). AMPAR/NMDAR ratios (Fig. 6A; Group X Cell Type, $F_{1,19}$=0.39, P=0.54), sEPSC

frequency (Fig. 6B; Group X Cell Type, $F_{1,73}$=1.75, P=0.19) and amplitude (Fig. 6C; Group X Cell Type, $F_{1,73}$=0.74, P=0.39), and PPRs (Fig. 6D; Stimulus Interval X Group X Cell Type $F_{6,156}$=0.38, P=0.89) were not modulated in S1.

Equally, following S11 we measured no significant interaction for AMPAR/NMDAR ratios (Fig. 6A; Group X Cell Type, $F_{1,19}$=0.01, P=0.92), although there was a main effect of Cell Type ($F_{1,19}$=5.66, P<0.05). Furthermore, we found no interaction effects for the sEPSC frequency (Fig. 6B; Group X Cell Type $F_{1,76}$=0.20, P=0.66), amplitude (Fig. 6C; Group X Cell Type $F_{1,76}$=0.05, P=0.83). However, we detected a main effect of Cell Type on the sEPSC frequency (Cell Type $F_{1,76}$=12.41, P<0.001). This frequency alteration was not due to changes in presynaptic function (Fig. 6D; Stimulus Interval X Group X Cell Type, $F_{6,150}$=1.01, P=0.42).

Connectivity changes are not observed in neurons activated in S1 and S11

Increased connectivity between neurons is thought to facilitate the establishment of CS-US representations (Choi et al., 2018; Ryan et al., 2015). We thus targeted GFP+ and GFP– neurons with paired electrophysiological recordings to determine whether appetitive conditioning increased ensemble connectivity. We analyzed the probability of a connection between GFP+ to GFP+ (+/+), GFP+ to GFP– (+/-) and GFP– to GFP+ (-/+) neurons across groups on S1 and S11 (Fig. 7A). Average connectivity probability was 9.88% between pyramidal pairs, in line with previous reports (Markram et al., 1997). We observed no change in connection probability between any neuron type in S1 and S11 (Fisher's Exact Test; Group X Connection, S1: +/+ P=0.61, +/- P=0.23, -/+ P=0.34; S11: +/+ P=1.00, +/- P=1.00, -/+ P=1.00; Fig. 7B).

Persistent excitability enhancement of S1-activated neurons impairs learning.

Neurons activated during S1 were hyper-excitable when mice did not exhibit cue-selective food seeking. To examine their behavioral role, we tagged neurons activated during S1 with the excitatory DREADD 'hM3Dq' in *Fos-tTA* mice using the TetTag DREADD approach (Figs. 8A, 8B) (Zhang et al., 2015). We repeatedly activated these tagged neurons using systemic injections of the hM3Dq agonist 'clozapine' (0.1 mg/kg) (Gomez et al., 2017) to artificially enhance excitability throughout

conditioning. This compound is a metabolite of the widely-used hM3Dq agonist clozapine-*N*-oxide, and has recently been shown to serve as the agonist at hM3Dq *in vivo* (Gomez et al., 2017). *Fos-tTA* mice and control wild-type (WT) mice not tagged with hM3Dq underwent acquisition and recall test sessions as before.

During acquisition (Fig 8D), there was a significant interaction effect of Cue X Session ($F_{11,176}$=6.94, P<0.001) and a significant effect of Cue during Recall (Fig. 8E; $F_{1,16}$=9.03, P<0.01) on discriminated approach performance. Moreover, we observed a significant interaction effect of Cue X Session X hM3Dq ($F_{11,176}$=2.00, P<0.05) on the number of responses (Fig. 8D). As before, we calculated the 'Selectivity Index' (Fig. 8C) and found a significant interaction of hM3Dq X Session ($F_{11,176}$=3.81, P<0.001) and post-hoc testing revealed significantly decrease cue-selective responding in *Fos-tTA* mice on a number of sessions (P<0.05). Thus, persistently enhancing the excitability of S1-activated neurons interfered with conditioning. During the test for recall, we observed a near significant interaction of hM3Dq X Cue (Fig. 8E; $F_{1,16}$=3.82, P=0.068) on the number of approach responses.

To confirm that these effects were relevant to S1-activated neurons, we repeatedly enhanced the excitability of neurons tagged following exposure to a neutral, novel context (NC) exposure (Fig. 8F). The exposure procedure activates neurons that are distinct from those activated by discrete (would-be) appetitive cues (Cruz et al., 2013; Fanous et al., 2012). We observed a significant interaction effect of Cue X Session on approach responses during acquisition ($F_{11,176}$= 5.19, P<0.001) and a significant effect of Cue during recall ($F_{1,16}$=45.53, P<0.001; Fig. 8H), again indicating robust conditioning in our procedure. However, we observed no significant effect of hM3Dq in acquisition (Fig. 8G) on the number of approach responses, and analysis of the Selectivity Index also revealed no significant interaction effect of hM3Dq X Session ($F_{11,176}$=0.32, P=0.97; Fig. 8F). Furthermore, we did not observe a significant interaction effect of hM3Dq X Cue on the number of responses during recall (Fig. 8H; $F_{1,16}$=0.32, P=0.88). Thus, in contrast to S1-tagged neurons, persistently enhancing the excitability of NC-tagged neurons did not affect conditioning.

Of note, all sessions in which clozapine was delivered were performed in the afternoon, closer to feeding time. We have previously observed in our that PM sessions often show poorer response selectivity than AM session in our task (Fig. 1C). Thus, while we did observe decreased performances at sessions 2, 4, 6, 8, 10, 12, this is not likely due to clozapine delivery.

Discussion

We show that the establishment of a CS-US association and cue-selective food-seeking, is associated with the recruitment of a stable, repeatedly activated subset of pyramidal cells in the dmPFC from a wider pool of neurons activated in the initial conditioning session (S1), when mice did not exhibit cue-selective food-seeking. A minority (29%) of pyramidal cells from this wider pool of candidate neurons were recruited into this ensemble. This recruitment was indicated by consistent reactivation across conditioning and in memory recall. S1-activated neurons exhibited hyper-excitability, which was not observed at later stages of conditioning when mice acquired cue-selective food seeking. Repeatedly enhancing the excitability of S1-tagged neurons during conditioning disrupted acquisition of a cue-discriminated appetitive performance. We provide novel insights into neuronal ensemble formation and how they may encode cue-evoked appetitive memories that control food seeking. Moreover, we identify a potential mechanism that determines which neurons become incorporated to form these ensembles.

Appetitive memory formation recruits a stable group of pyramidal cells from the initial conditioning session

CS-activated neurons are a small subset (~6-12%) of the total neuronal population (Bossert et al., 2011; Fanous et al., 2012), and their selective silencing in the mPFC disrupts reward seeking, indicating their role in CS-US memory encoding (Bossert et al., 2011; Suto et al., 2016). However, these studies did not examine whether a subgroup of these neurons were repeatedly activated during learning. During CS-evoked memory recall, we revealed increased recruitment of a pyramidal cell ensemble that exhibited a stable activation history during conditioning, suggesting its role in cue-selective food seeking. These stably activated neurons were originally recruited in the initial conditioning session, and that activation history may influence their inclusion into a conditioning ensemble. Moreover, only 23% of neurons activated during memory recall exhibited persistent activation throughout acquisition. Our findings illuminate how a subgroup of neurons within a population of CS-activated neurons may encode a CS-US memory. They raise the intriguing possibility that methods which manipulate appetitive behaviors by silencing CS-activated neurons (Suto et al., 2016) may exert their effects through such a neuronal subgroup with a repeated learning

activation history. However, the tools to selectively manipulate this subgroup in order to confirm this idea are currently unavailable. Finally, in general, more neurons were persistently activated in all sessions compared to neurons activated in mid and late, but not early conditioning, a similar pattern also observed in Recall-activated neurons. Since mPFC neurons participate in contextual encoding during exploration (Hyman et al., 2012), such persistently activated neurons may encode environmental features of the training context following its repeated exposure.

We did not observe the enhanced recruitment of a repeatedly activated subset of interneurons during conditioning and memory recall (Fig. 4C, F). However, we did observe an increased reactivation likelihood following S1 at an overall population level (Fig. 4D, G). These seemingly discrepant findings may arise from individual variability across mice, which the population analysis does not consider. Also, we did not account for the various interneuron subclasses with different functional characteristics, which exhibit differential activity during food-seeking (Gaykema et al., 2014). Moreover, in the hippocampus certain interneuron subclasses are recruited during learning and regulate excitatory ensemble recruitment (Stefanelli et al., 2016), and hippocampal interneurons exhibit excitability alterations following conditioning (McKay et al., 2013). Additional work is necessary to elucidate the role of specific dmPFC interneuron subtypes and their excitability alterations during appetitive conditioning.

Conditioning-related parameters modulate the excitability of behaviorally-activated neurons

We identified a hyper-excitable pool of pyramidal cells activated on the initial, but not late conditioning session in Paired mice. These excitability alterations might be related to temporally contiguous CS and US presentations, as they were not observed in GFP+ neurons of Unpaired mice that received CS and US presentations at disparate times. Currently, we cannot rule out if this hyper-excitability was present prior to S1. Therefore in Paired mice, a pre-existing elevated baseline excitability may have rendered certain neurons to become activated in S1 and thus express GFP (Gouty-Colomer et al., 2016; Yiu et al., 2014).

The hyper-excitability in *Fos-GFP* mice following conditioning was observed several hours after behavioral testing. This prolonged excitability increase may induce long-term plasticity which function to promote memory consolidation following the conditioning session, by facilitating ensemble reactivation that occurs many hours following training (de Sousa et al., 2019). An interesting future investigation is to determine how a baseline or training-induced hyper-excitability of dmPFC S1-activated neurons influences ensemble recruitment. However, a direct link between such hyper-excitability and ensemble recruitment is difficult to establish. Currently, we cannot identify and measure the excitability in vivo from those S1-activated neurons that will become recruited to the ensemble throughout conditioning. Nevertheless, the proposed roles of hyper-excitability in memory and our imaging findings raise the possibility that the stable conditioning-related ensemble emerges from a hyper-excitable neuronal pool activated in the initial conditioning session.

Implications of excitability alterations on behaviorally-activated neurons

Chemogenetically enhancing the excitability of the neuronal pool activated in S1 throughout conditioning interfered with mice acquiring a reliable cue-evoked food-seeking response. Thus, the dissipation of neuronal hyper-excitability may be necessary to acquire robust cue-evoked food seeking. However, in a study by Volle et al. (2016), increasing mPFC hyper-excitability using widespread hM3Dq expression resulted in potentiated trace conditioning. They proposed that this manipulation facilitated animals to acquire low-grade associations (e.g. under conditions of low temporal contiguity or poor contingency) that would otherwise fail to support robust learning. Therefore, our mice with enhanced excitability may have learned relevant, but also irrelevant or spurious associations between the US and other stimuli (or interoceptive events), leading to disrupted discriminative performance. In support, lesion studies suggest the dmPFC promotes the formation of relevant and precise associations that enable proper cue discrimination (Bussey et al., 1997; Cardinal et al., 2002; Parkinson et al., 2000). Although we used activity-based tagging, our DREADD manipulation was not cell-type specific. However, we observed that the vast majority of GFP+ neurons were pyramidal cells (Fig. 3D), consistent with our recent study (Ziminski et al., 2017).

From a behavior ecology perspective, Macarthur and Pianka theorized that animals would tend towards optimal foraging behaviors in which they minimize time and energy spent food seeking (MacArthur and Pianka, 1966). In our learning task, this is related to reduced non-specific responses (i.e. high selectivity index). We observed attenuated selectivity and high non-selective responses following repeated chemogenetic excitability enhancements of S1-activated neurons. Collectively, we theorize that early conditioning activates a hyper-excitable neuronal pool in the dmPFC to facilitate the selection of neurons into a stable ensemble that eventually supports a robust CS-US association. Given the role of the dmPFC in attention and motivation (Bryden et al., 2011; Cardinal et al., 2002; Parkinson et al., 2000; Totah et al., 2009), neuronal hyper-excitability helps engage these processes during initial CS-US formation. However, this hyper-excitability non-selectively amplifies environmental stimuli and decreases the signal-to-noise ratio of extracted information. Therefore, this excitability needs to renormalize during the transition from non-selective to selective responding to food cues, to promote to optimal food-seeking.

No observed learning-relevant changes in synaptic properties and connectivity

We observed no selective learning-induced changes in the synaptic strength nor connectivity of activated neurons, in contrast to other observations following establishment of aversive associations (Choi et al., 2018; Gouty-Colomer et al., 2016; Ryan et al., 2015). Several factors may have contributed to this difference. First, mice received sucrose under food-restriction, which can induce synaptic strength alterations (Peng et al., 2015). We observed decreases in AMPAR/NMDAR ratios and sEPSC frequency in GFP+ neurons in Paired and Unpaired mice at S11. Thus, synaptic alterations in neurons repeatedly activated by sucrose may have masked learning-related synaptic adaptations that contribute to stable ensemble formation. Also, mPFC synaptic changes may not occur immediately following learning, but develop later in a hippocampal-dependent process (Restivo et al., 2009). Thus, a prolonged delay following appetitive learning (e.g. weeks) that is associated with memory engram maturation (Kitamura et al., 2017) may better reveal learning-selective synaptic changes. Finally, recent studies have demonstrated learning-induced increases in ensemble intra-connectivity by using optogenetic ensemble stimulation in one brain area while recording from a target ensemble neurons in another (Choi et al., 2018; Ryan et al., 2015). Our lack

of observed connectivity changes may be due to utilization of paired recordings, in which connections between individual activated neurons were locally assessed rather than across two different brain areas.

Conclusion and future directions

Despite appetitive conditioning's importance in survival, few studies have established its precise mechanisms at the neuronal ensemble level in the mPFC. We provide the initial key evidence regarding dmPFC ensemble recruitment and corresponding excitability alterations that reflect different stages of optimal food-seeking. Further investigations are necessary to determine which hyper-excitable neurons activated early in our conditioning procedure will become allocated to the CS-US ensemble. Hence, tools to measure neuronal excitability and recruitment *in vivo* need to be developed to identify the properties that determine this recruitment process. This will allow us to better grasp the principles that govern neuronal ensemble recruitment and its alterations for establishing associative memories.

References

van den Akker, K., Schyns, G., and Jansen, A. (2018). Learned Overeating: Applying Principles of Pavlovian Conditioning to Explain and Treat Overeating. Curr Addict Rep *5*, 223–231.

Barth, A.L., Gerkin, R.C., and Dean, K.L. (2004). Alteration of Neuronal Firing Properties after In Vivo Experience in a FosGFP Transgenic Mouse. J. Neurosci. *24*, 6466–6475.

Beasley, T.M., and Schumacker, R.E. (1995). Multiple Regression Approach to Analyzing Contingency Tables: Post Hoc and Planned Comparison Procedures. The Journal of Experimental Education *64*, 79–93.

Besser, S., Sicker, M., Marx, G., Winkler, U., Eulenburg, V., Hülsmann, S., and Hirrlinger, J. (2015). A Transgenic Mouse Line Expressing the Red Fluorescent Protein tdTomato in GABAergic Neurons. PLOS ONE *10*, e0129934.

Bolte, S., and Cordelières, F.P. (2006). A guided tour into subcellular colocalization analysis in light microscopy. J Microsc *224*, 213–232.

Bossert, J.M., Stern, A.L., Theberge, F.R.M., Cifani, C., Koya, E., Hope, B.T., and Shaham, Y. (2011). Ventral medial prefrontal cortex neuronal ensembles mediate context-induced relapse to heroin. Nat. Neurosci. *14*, 420–422.

Bryden, D.W., Johnson, E.E., Tobia, S.C., Kashtelyan, V., and Roesch, M.R. (2011). Attention for Learning Signals in Anterior Cingulate Cortex. J. Neurosci. *31*, 18266–18274.

Bussey, T.J., Everitt, B.J., and Robbins, T.W. (1997). Dissociable effects of cingulate and medial frontal cortex lesions on stimulus-reward learning using a novel Pavlovian autoshaping procedure for the rat: implications for the neurobiology of emotion. Behav. Neurosci. *111*, 908–919.

Cao, V.Y., Ye, Y., Mastwal, S., Ren, M., Coon, M., Liu, Q., Costa, R.M., and Wang, K.H. (2015). Motor Learning Consolidates Arc-Expressing Neuronal Ensembles in Secondary Motor Cortex. Neuron *86*, 1385–1392.

Cao, X.-Y., Xu, H., Wu, L.-J., Li, X.-Y., Chen, T., and Zhuo, M. (2009). Characterization of intrinsic properties of cingulate pyramidal neurons in adult mice after nerve injury. Mol Pain *5*, 73.

Cardinal, R.N., Parkinson, J.A., Lachenal, G., Halkerston, K.M., Rudarakanchana, N., Hall, J., Morrison, C.H., Howes, S.R., Robbins, T.W., and Everitt, B.J. (2002). Effects of selective excitotoxic lesions of the nucleus accumbens core, anterior cingulate cortex, and central nucleus of the amygdala on autoshaping performance in rats. Behav. Neurosci. *116*, 553–567.

Carthey, A.J.R., Bytheway, J.P., and Banks, P.B. (2011). Negotiating a noisy, information-rich environment in search of cryptic prey: olfactory predators need patchiness in prey cues. J Anim Ecol *80*, 742–752.

Choi, J.-H., Sim, S.-E., Kim, J., Choi, D.I., Oh, J., Ye, S., Lee, J., Kim, T., Ko, H.-G., Lim, C.-S., et al. (2018). Interregional synaptic maps among engram cells underlie memory formation. Science *360*, 430–435.

Cifani, C., Koya, E., Navarre, B.M., Calu, D.J., Baumann, M.H., Marchant, N.J., Liu, Q.-R., Khuc, T., Pickel, J., Lupica, C.R., et al. (2012). Medial Prefrontal Cortex Neuronal Activation and Synaptic Alterations after Stress-Induced Reinstatement of Palatable Food Seeking: A Study Using c-fos-GFP Transgenic Female Rats. J. Neurosci. *32*, 8480–8490.

Cruz, F.C., Koya, E., Guez-Barber, D.H., Bossert, J.M., Lupica, C.R., Shaham, Y., and Hope, B.T. (2013). New technologies for examining the role of neuronal ensembles in drug addiction and fear. Nat. Rev. Neurosci. *14*, 743–754.

Cruz, F.C., Babin, K.R., Leao, R.M., Goldart, E.M., Bossert, J.M., Shaham, Y., and Hope, B.T. (2014). Role of Nucleus Accumbens Shell Neuronal Ensembles in Context-Induced Reinstatement of Cocaine-Seeking. J. Neurosci. *34*, 7437–7446.

Fanous, S., Goldart, E.M., Theberge, F.R.M., Bossert, J.M., Shaham, Y., and Hope, B.T. (2012). Role of orbitofrontal cortex neuronal ensembles in the expression of incubation of heroin craving. J. Neurosci. *32*, 11600–11609.

Gaykema, R.P.A., Nguyen, X.-M.T., Boehret, J.M., Lambeth, P.S., Joy-Gaba, J., Warthen, D.M., and Scott, M.M. (2014). Characterization of excitatory and inhibitory neuron activation in the mouse medial prefrontal cortex following palatable food ingestion and food driven exploratory behavior. Front Neuroanat *8*.

Gomez, J.L., Bonaventura, J., Lesniak, W., Mathews, W.B., Sysa-Shah, P., Rodriguez, L.A., Ellis, R.J., Richie, C.T., Harvey, B.K., Dannals, R.F., et al. (2017). Chemogenetics revealed: DREADD occupancy and activation via converted clozapine. Science *357*, 503–507.

Gouty-Colomer, L.A., Hosseini, B., Marcelo, I.M., Schreiber, J., Slump, D.E., Yamaguchi, S., Houweling, A.R., Jaarsma, D., Elgersma, Y., and Kushner, S.A. (2016). *Arc* expression identifies the lateral amygdala fear memory trace. Molecular Psychiatry *21*, 364–375.

Guzman, S.J., Schlögl, A., and Schmidt-Hieber, C. (2014). Stimfit: quantifying electrophysiological data with Python. Front Neuroinform *8*, 16.

Hyman, J.M., Ma, L., Balaguer-Ballester, E., Durstewitz, D., and Seamans, J.K. (2012). Contextual encoding by ensembles of medial prefrontal cortex neurons. PNAS *109*, 5086–5091.

Ishikawa, M., Mu, P., Moyer, J.T., Wolf, J.A., Quock, R.M., Davies, N.M., Hu, X. -t., Schluter, O.M., and Dong, Y. (2009). Homeostatic Synapse-Driven Membrane Plasticity in Nucleus Accumbens Neurons. Journal of Neuroscience *29*, 5820–5831.

Jansen, A. (1998). A learning model of binge eating: cue reactivity and cue exposure. Behav Res Ther *36*, 257–272.

Kitamura, T., Ogawa, S.K., Roy, D.S., Okuyama, T., Morrissey, M.D., Smith, L.M., Redondo, R.L., and Tonegawa, S. (2017). Engrams and Circuits Crucial for Systems Consolidation of a Memory. Science *356*, 73–78.

Koya, E., Uejima, J.L., Wihbey, K.A., Bossert, J.M., Hope, B.T., and Shaham, Y. (2009). Role of ventral medial prefrontal cortex in incubation of cocaine craving. Neuropharmacology *56 Suppl 1*, 177–185.

Koya, E., Cruz, F.C., Ator, R., Golden, S.A., Hoffman, A.F., Lupica, C.R., and Hope, B.T. (2012). Silent synapses in selectively activated nucleus accumbens neurons following cocaine sensitization. Nature Neuroscience *15*, 1556–1562.

Low, R.J., Gu, Y., and Tank, D.W. (2014). Cellular resolution optical access to brain regions in fissures: Imaging medial prefrontal cortex and grid cells in entorhinal cortex. Proceedings of the National Academy of Sciences *111*, 18739–18744.

MacArthur, R.H., and Pianka, E.R. (1966). On Optimal Use of a Patchy Environment. The American Naturalist *100*, 603–609.

Markram, H., Lübke, J., Frotscher, M., Roth, A., and Sakmann, B. (1997). Physiology and anatomy of synaptic connections between thick tufted pyramidal neurones in the developing rat neocortex. J. Physiol. (Lond.) *500 (Pt 2)*, 409–440.

Mattson, B.J., Koya, E., Simmons, D.E., Mitchell, T.B., Berkow, A., Crombag, H.S., and Hope, B.T. (2008). Context-specific sensitization of cocaine-induced locomotor activity and associated neuronal ensembles in rat nucleus accumbens. Eur. J. Neurosci. *27*, 202–212.

McKay, B.M., Oh, M.M., and Disterhoft, J.F. (2013). Learning increases intrinsic excitability of hippocampal interneurons. J. Neurosci. *33*, 5499–5506.

Parkinson, J.A., Willoughby, P.J., Robbins, T.W., and Everitt, B.J. (2000). Disconnection of the anterior cingulate cortex and nucleus accumbens core impairs Pavlovian approach behavior: further evidence for limbic cortical-ventral striatopallidal systems. Behav. Neurosci. *114*, 42–63.

Pavlov, I., P. (1927). Conditioned reflexes (Oxford, UK: Oxford University Press).

Paxinos, G., and Franklin, K. (2001). The mouse brain atlas in stereotaxic coordinates. San Diego, CA: Academic.

Peng, X.-X., Lister, A., Rabinowitsch, A., Kolaric, R., Cabeza de Vaca, S., Ziff, E.B., and Carr, K.D. (2015). Episodic sucrose intake during food restriction increases synaptic abundance of AMPA receptors in nucleus accumbens and augments intake of sucrose following restoration of ad libitum feeding. Neuroscience *295*, 58–71.

Pologruto, T.A., Sabatini, B.L., and Svoboda, K. (2003). ScanImage: Flexible software for operating laser scanning microscopes. BioMedical Engineering OnLine *2*, 13.

Restivo, L., Vetere, G., Bontempi, B., and Ammassari-Teule, M. (2009). The Formation of Recent and Remote Memory Is Associated with Time-Dependent Formation of Dendritic Spines in the Hippocampus and Anterior Cingulate Cortex. Journal of Neuroscience *29*, 8206–8214.

Riebe, I., Seth, H., Culley, G., Dósa, Z., Radi, S., Strand, K., Fröjd, V., and Hanse, E. (2016). Tonically active NMDA receptors – a signalling mechanism critical for interneuronal excitability in the CA1 stratum radiatum. European Journal of Neuroscience *43*, 169–178.

Riga, D., Matos, M.R., Glas, A., Smit, A.B., Spijker, S., and Van den Oever, M.C. (2014). Optogenetic dissection of medial prefrontal cortex circuitry. Front Syst Neurosci *8*, 230.

Ryan, T.J., Roy, D.S., Pignatelli, M., Arons, A., and Tonegawa, S. (2015). Engram cells retain memory under retrograde amnesia. Science *348*, 1007–1013.

Schindelin, J., Arganda-Carreras, I., Frise, E., Kaynig, V., Longair, M., Pietzsch, T., Preibisch, S., Rueden, C., Saalfeld, S., Schmid, B., et al. (2012). Fiji: an open-source platform for biological-image analysis. Nat. Methods *9*, 676–682.

de Sousa, A.F., Cowansage, K.K., Zutshi, I., Cardozo, L.M., Yoo, E.J., Leutgeb, S., and Mayford, M. (2019). Optogenetic reactivation of memory ensembles in the retrosplenial cortex induces systems consolidation. Proc. Natl. Acad. Sci. U.S.A. *116*, 8576–8581.

Stefanelli, T., Bertollini, C., Lüscher, C., Muller, D., and Mendez, P. (2016). Hippocampal Somatostatin Interneurons Control the Size of Neuronal Memory Ensembles. Neuron *89*, 1074–1085.

Suto, N., Laque, A., De Ness, G.L., Wagner, G.E., Watry, D., Kerr, T., Koya, E., Mayford, M.R., Hope, B.T., and Weiss, F. (2016). Distinct memory engrams in the infralimbic cortex of rats control opposing environmental actions on a learned behavior. ELife *5*.

Takeuchi, T., Duszkiewicz, A.J., and Morris, R.G.M. (2014). The synaptic plasticity and memory hypothesis: encoding, storage and persistence. Philos. Trans. R. Soc. Lond., B, Biol. Sci. *369*, 20130288.

Tayler, K.K., Tanaka, K.Z., Reijmers, L.G., and Wiltgen, B.J. (2013). Reactivation of neural ensembles during the retrieval of recent and remote memory. Curr. Biol. *23*, 99–106.

Thevenaz, P., Ruttimann, U.E., and Unser, M. (1998). A pyramid approach to subpixel registration based on intensity. IEEE Transactions on Image Processing *7*, 27–41.

Ting, J.T., Daigle, T.L., Chen, Q., and Feng, G. (2014). Acute brain slice methods for adult and aging animals: application of targeted patch clamp analysis and optogenetics. Methods Mol. Biol. *1183*, 221–242.

Totah, N.K.B., Kim, Y.B., Homayoun, H., and Moghaddam, B. (2009). Anterior cingulate neurons represent errors and preparatory attention within the same behavioral sequence. J. Neurosci. *29*, 6418–6426.

Tumbar, T., Guasch, G., Greco, V., Blanpain, C., Lowry, W.E., Rendl, M., and Fuchs, E. (2004). Defining the epithelial stem cell niche in skin. Science *303*, 359–363.

Whitaker, L.R., and Hope, B.T. (2018). Chasing the addicted engram: identifying functional alterations in Fos-expressing neuronal ensembles that mediate drug-related learned behavior. Learn. Mem. *25*, 455–460.

Whitaker, L.R., Carneiro de Oliveira, P.E., McPherson, K.B., Fallon, R.V., Planeta, C.S., Bonci, A., and Hope, B.T. (2016). Associative Learning Drives the Formation of Silent Synapses in Neuronal Ensembles of the Nucleus Accumbens. Biol. Psychiatry *80*, 246–256.

Whitaker, L.R., Warren, B.L., Venniro, M., Harte, T.C., McPherson, K.B., Beidel, J., Bossert, J.M., Shaham, Y., Bonci, A., and Hope, B.T. (2017). Bidirectional Modulation of Intrinsic Excitability in Rat Prelimbic Cortex Neuronal Ensembles and Non-Ensembles after Operant Learning. J. Neurosci. *37*, 8845–8856.

Zhang, Z., Ferretti, V., Güntan, İ., Moro, A., Steinberg, E.A., Ye, Z., Zecharia, A.Y., Yu, X., Vyssotski, A.L., Brickley, S.G., et al. (2015). Neuronal ensembles sufficient for recovery sleep and the sedative actions of α2 adrenergic agonists. Nat. Neurosci. *18*, 553–561.

Ziminski, J.J., Hessler, S., Margetts-Smith, G., Sieburg, M.C., Crombag, H.S., and Koya, E. (2017). Changes in Appetitive Associative Strength Modulates Nucleus Accumbens, But Not Orbitofrontal Cortex Neuronal Ensemble Excitability. J. Neurosci. *37*, 3160–3170.

Figures and legends

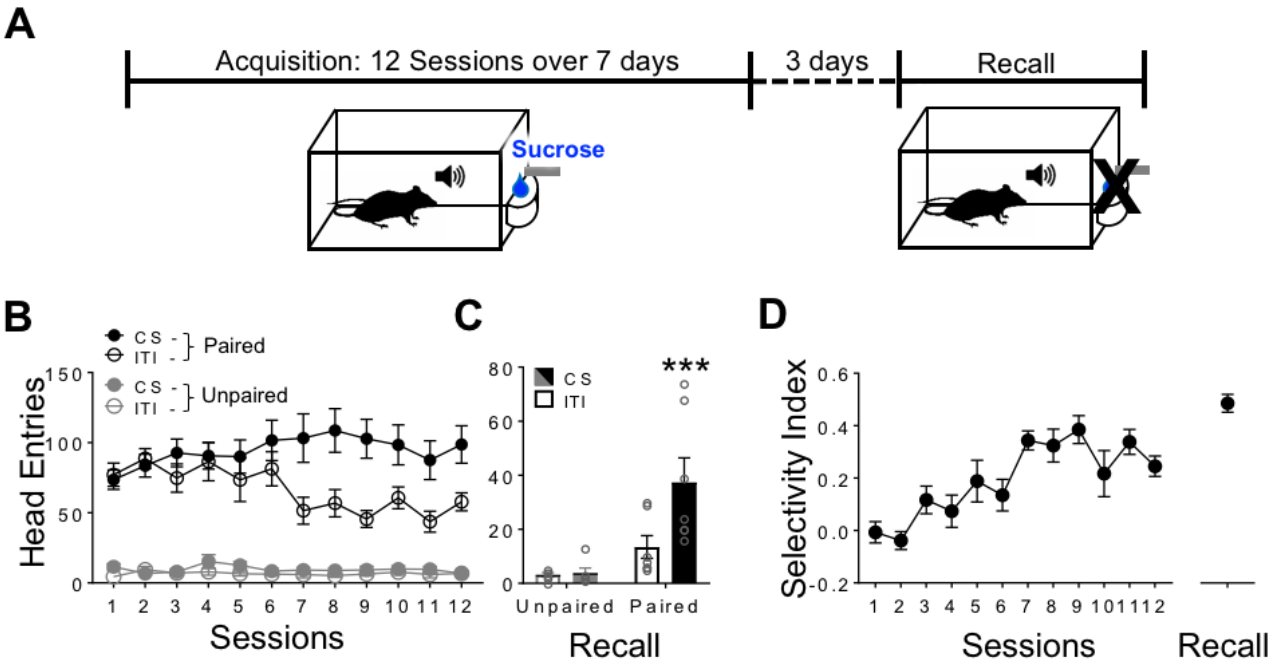

Figure 1

Figure 1: Experimental timeline and conditioned approach performance in FGGT mice. (A) Timeline of conditioning and imaging sessions (1-2 sessions per day). **(B)** Head entries into the magazine during the CS (cue-on) compared to ITI (no cue) periods as a function of conditioning session. **(C)** Approach responses during CS and ITI trials during the test for recall by Paired and Unpaired groups. **(D)** 'Selectivity index' (CS-ITI/total number head entries) of Paired mice during Acquisition and Recall. All data are expressed as Mean±SEM *** *P<0.001; Paired (P) n=12, Unpaired (UP) n=10. Paired (P) n=6, Unpaired (UP) n=6 for Recall.*

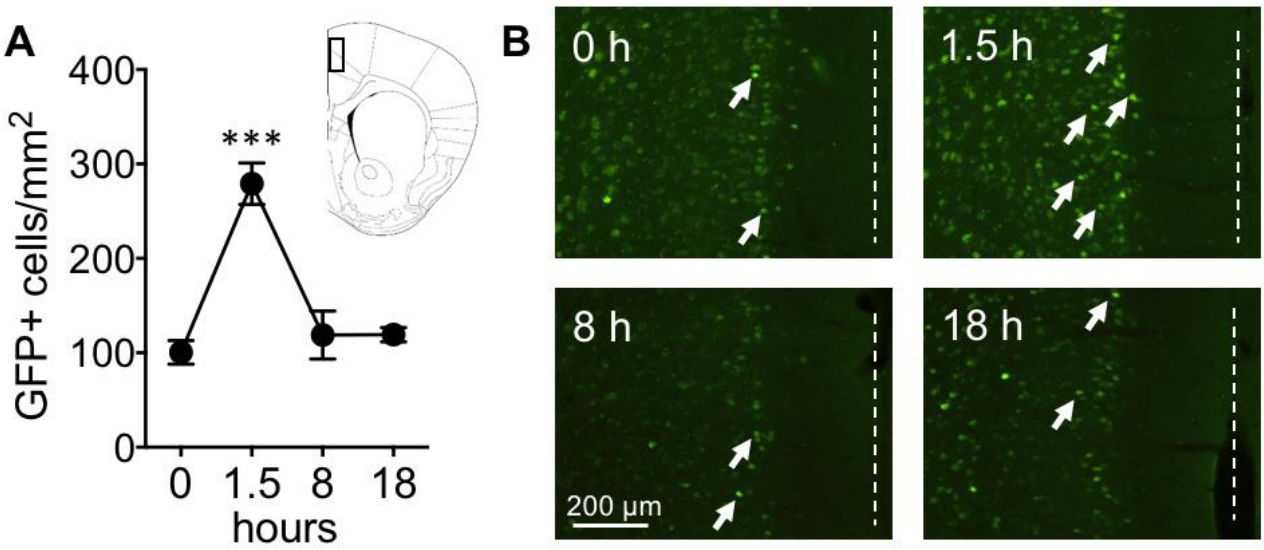
A
400
300
200
100
0
GFP+ cells/mm2
***
0 1.5 8 18
hours
B
0 h
1.5 h
8 h
18 h
200 µm

Figure 2

Figure 2: dmPFC Fos-GFP expression peaks at 1.5 h and returns to baseline at 8 and 18 h. **(A)** Time course of Fos-GFP expression and approximate location of cell counts. Data are from naïve *Fos-GFP* mice that were perfused at 0, 1.5, 8, and 18 h following exposure to a novel context. **(B)** Representative images of Fos-GFP labeling from the dmPFC. White arrows indicate Fos-GFP+ cells and dashed white line indicates position of midline. All data are expressed as Mean±SEM *** *P<0.001 (n=5,5,5,4 mice for 0, 1.5, 8, and 18 h groups, respectively)*

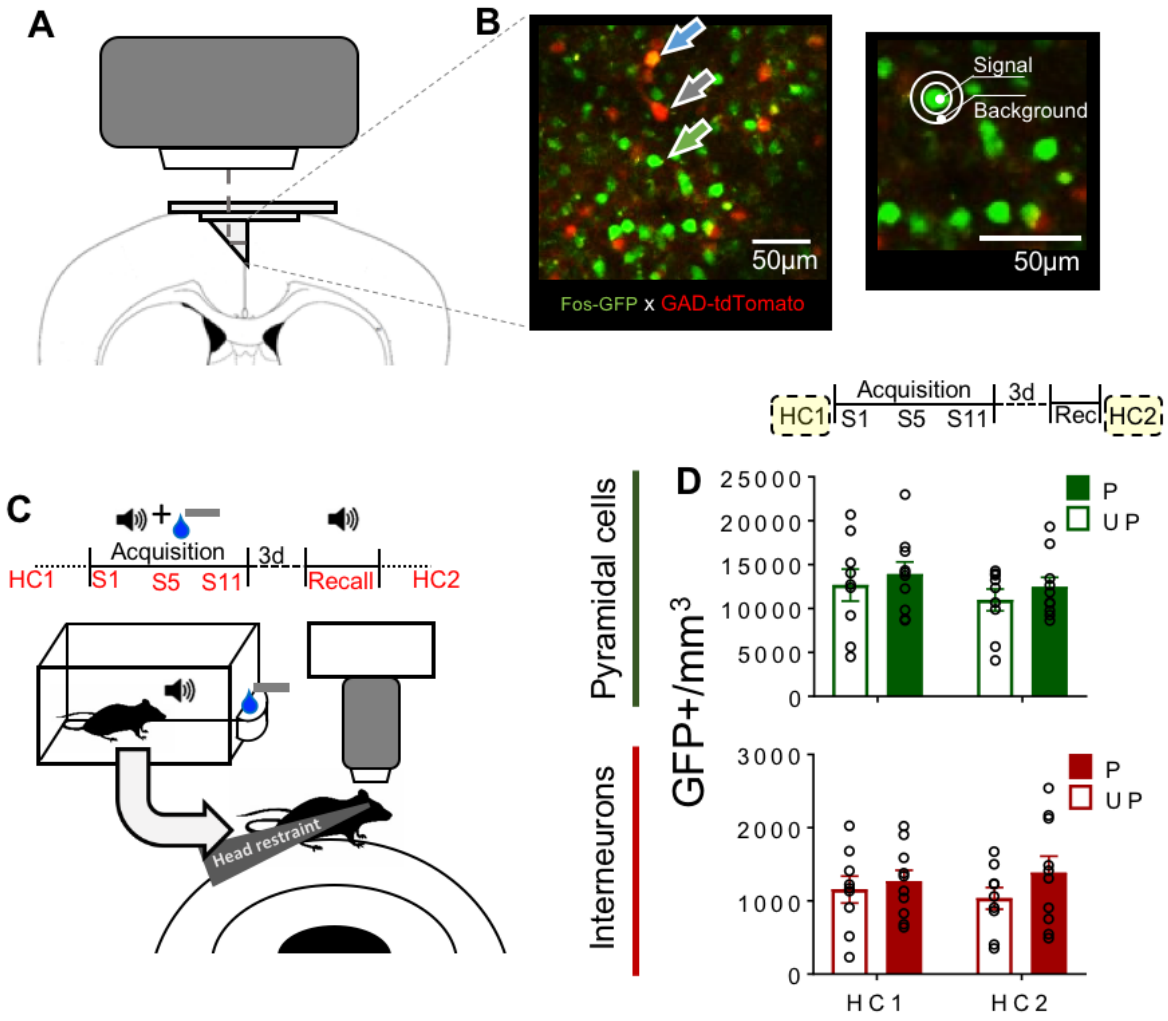
A
B
50µm
Fos-GFP x GAD-tdTomato
Signal
Background
50µm
HC1
Acquisition
S1
S5
S11
3d
Rec
HC2
C
Acquisition
3d
HC1
S1
S5
S11
Recall
HC2
Head restraint
D
Pyramidal cells
Interneurons
GFP+/mm3
25000
20000
15000
10000
5000
0
3000
2000
1000
P
UP
HC1
HC2

Figure 3

Figure 3: Experimental timeline, methods of 2-Photon imaging, and baseline Fos-GFP expression. GFP expression was longitudinally monitored in pyramidal cells and interneurons. **(A)** Microprism placement for dmPFC imaging. **(B**) Representative *in vivo* 2-Photon image of dmPFC from *Fos-GFP x GAD-tdTomato (FGGT)* mice (green arrow: GFP; grey arrow: tdTomato; blue arrow: GFP+tdTomato). GFP+ neurons were selected by comparing 'Signal' intensity to 'Background'. **(C)** Imaging timeline and schematic representation of imaging session in head-fixed mice following behavioral training under freely moving conditions (S1, S5, S11 and Recall) or from home cage (HC1, HC2). **(D)** Number of GFP+ pyramidal cells (green) and interneurons (red) per mm^3 in imaging sessions taking place directly from home cage both before (HC1) and after (HC2) behavioral training. All data are expressed as Mean±SEM. *Paired (P) n=10, Unpaired (UP) n=9*.

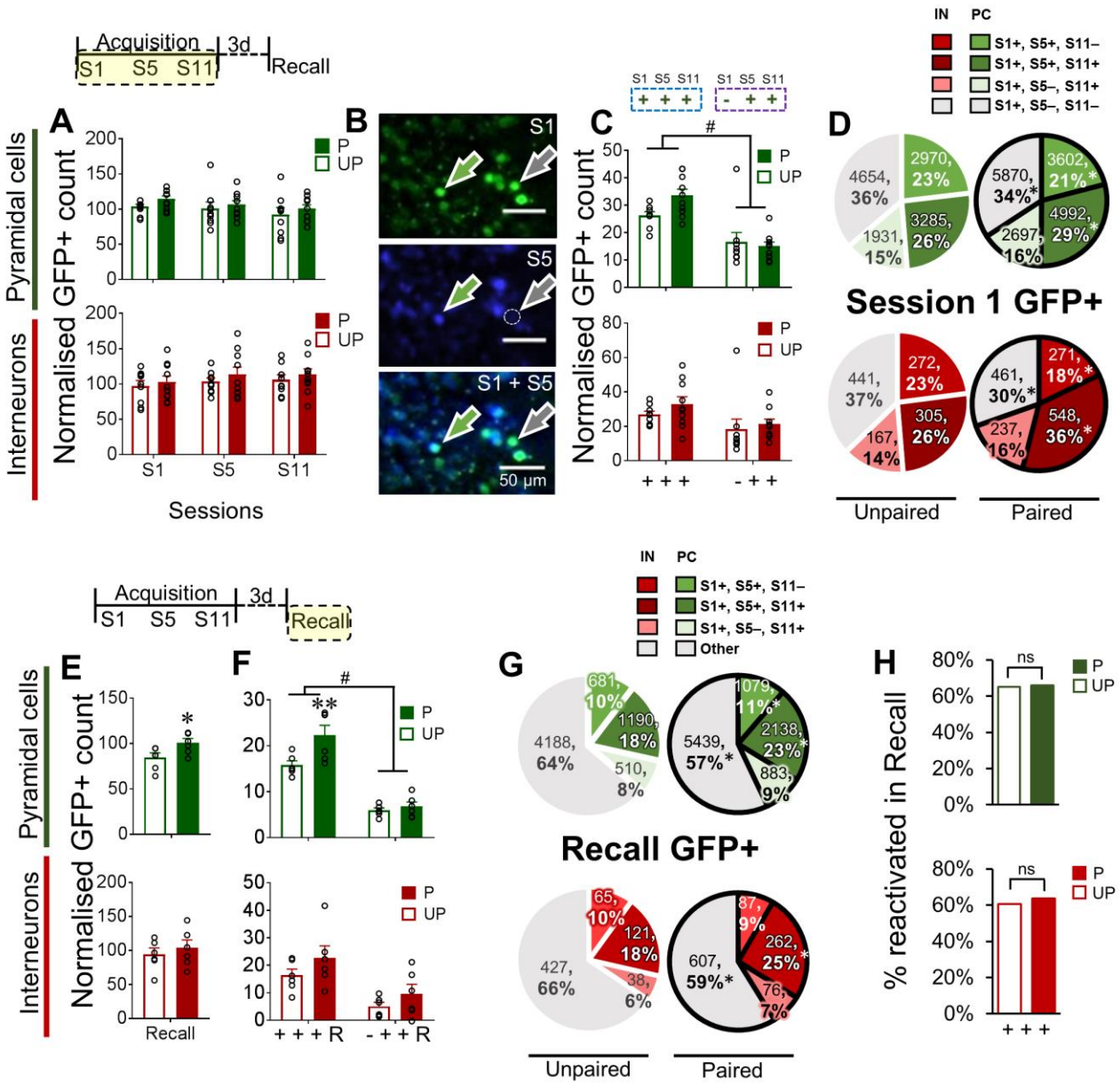
Acquisition
3d
Recall
S1 S5 S11
A
B
C
D
Pyramidal cells
Interneurons
Normalised GFP+ count
P
UP
S1
S5
S11
Sessions
S1 + S5
50 µm
#
IN
PC
S1+, S5+, S11–
S1+, S5+, S11+
S1+, S5–, S11+
S1+, S5–, S11–
Session 1 GFP+
Unpaired
Paired
E
F
G
H
Other
Recall GFP+
% reactivated in Recall
ns

Figure 4

Figure 4: Conditioning and memory recall recruits a stable pyramidal cell ensemble from the initial acquisition session. (A) Normalized GFP+ counts of pyramidal cells (green) and interneurons (red) during acquisition sessions. **(B)** Representative image of longitudinal GFP imaging (S1 and S5); green arrow S1+|S5+ neurons, grey arrow S1+|S5- neurons. **(C)** Normalized GFP+ counts of pyramidal cells (PC) and interneurons (IN) with a S1 (+ + +) or no S1 (– + +) activation history. **(D)** Distribution of GFP+ pyramidal cells and interneurons activated during S1 classified according to their subsequent reactivation patterns (S1+|S5+,S11+; S1+|S5+, S11-; S1+|S5-, S11+; S1+|S5-,S11-) for Paired and Unpaired mice. **(E)** Normalized GFP+ counts of pyramidal cells and interneurons following the test for memory recall. **(F)** Normalized GFP+ counts of pyramidal cells and interneurons recruited during the test for recall that had been persistently activated during training, as a function of their S1 activation history (+ + + R or – + + R). **(G)** Distribution of GFP+ pyramidal cells (PC) and interneurons (IN) activated during the test for recall, classified according to their activation patterns from S1 onwards in Paired and Unpaired mice. 'Other' refers to neurons recruited during recall that did not demonstrate activation histories of interest (e.g. S1-|S5-, S11+). **(H)** Proportion of S1+|S5+ S11+ pyramidal cells and interneurons that were reactivated in Recall for Paired and Unpaired mice. Data on bar graphs are expressed as Mean±SEM. Normalization of GFP+ counts was performed using the average number of GFP+ neurons in HC (number of GFP+ cells / average number of GFP+ in HC) *100). *Interaction effect: # P<0.05*, *Post-hoc analysis: **P<0.01, Paired (P) n=10, Unpaired (UP) n=9 for acquisition, Paired (P) n=6, Unpaired (UP) n=6 for Recall.*

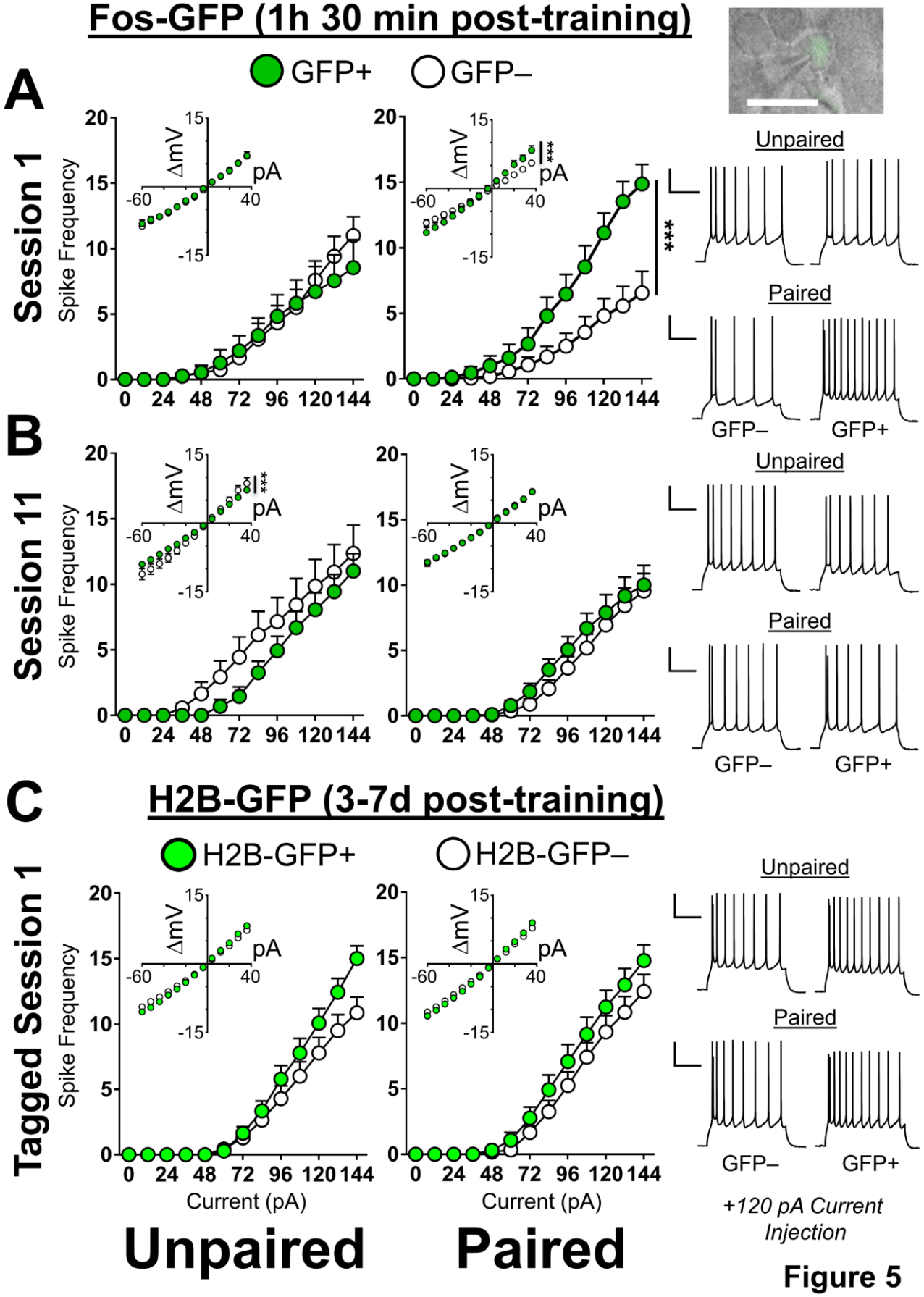
Fos-GFP (1h 30 min post-training)
GFP+
GFP–
A
Session 1
Spike Frequency
ΔmV
pA
***
Unpaired
Paired
GFP–
GFP+
B
Session 11
C
H2B-GFP (3-7d post-training)
H2B-GFP+
H2B-GFP–
Tagged Session 1
Current (pA)
Unpaired
Paired
+120 pA Current Injection

Figure 5

Figure 5. The firing capacity of S1-activated pyramidal cells is enhanced, but is not observed several days following S1 nor at S11.

(A) Following S1, GFP+ spike frequency is significantly higher than GFP– neurons in Paired, but not Unpaired mice (Paired; GFP+ n=5/15, GFP– n=5/16, Unpaired; GFP+ n=6/11, GFP– n=6/12). **(B)** Following S11, GFP+ and GFP– spike frequency is similar in both Paired and Unpaired mice (Paired; GFP+ n=6/19, GFP– n=6/17, Unpaired; GFP+ n=6/16, GFP– n=6/14)**.** Right top: Representative image of a patched GFP+ pyramidal cell in the dmPFC of a *Fos-GFP* mouse, scale bar 20 μm. Right: Representative traces from GFP+ and GFP– pyramidal cells of Paired and Unpaired mice at 120 pA stimulation. **(C)** The spike frequency of neurons activated at S1 of Acquisition returns to baseline 3-7d following training in *TetTag H2B-GFP* mice (Paired; H2B-GFP+ n=6/13, H2B-GFP– n=6/12), Unpaired; H2B-GFP+ n=6/14, H2B-GFP– n=6/14). Right: Representative traces from H2B-GFP+ and H2B-GFP– pyramidal cells of Paired and Unpaired mice at 120 pA stimulation, scale bars 25 mV, 250 ms. *Inset:* Current/voltage (I/V) curves. All data are expressed as Mean±SEM; *n*= number of animals/number of cells total. *** *indicates Two-way mixed ANOVA Cell Type X Current P<0.001.*

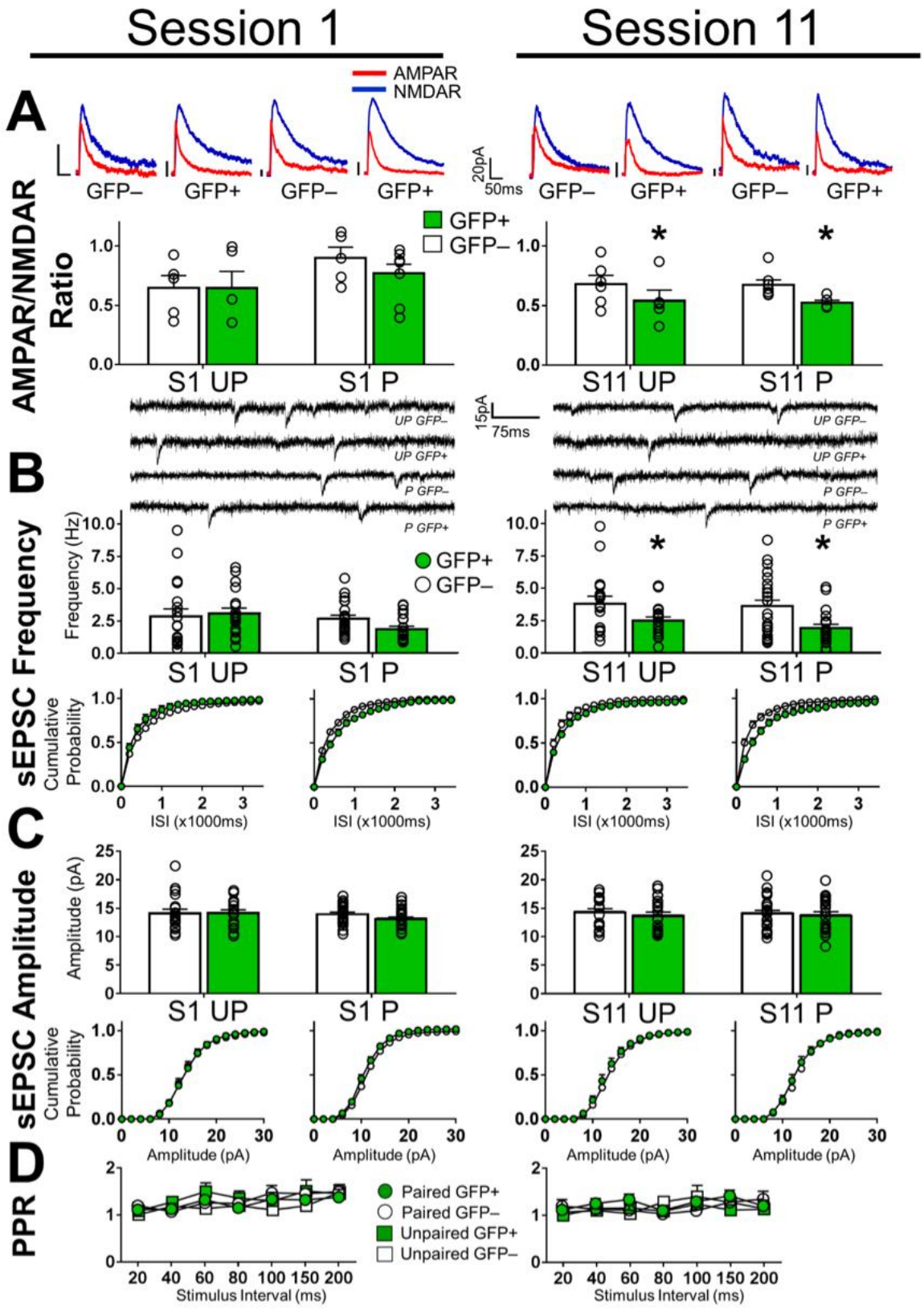
Session 1
Session 11
A
AMPAR
NMDAR
GFP–
GFP+
20pA
50ms
AMPAR/NMDAR Ratio
GFP+
GFP–
S1 UP
S1 P
S11 UP
S11 P
B
15pA
75ms
UP GFP–
UP GFP+
P GFP–
P GFP+
sEPSC Frequency
Frequency (Hz)
C
sEPSC Amplitude
Amplitude (pA)
Cumulative Probability
ISI (x1000ms)
D
PPR
Paired GFP+
Paired GFP–
Unpaired GFP+
Unpaired GFP–
Stimulus Interval (ms)

Figure 6

Figure 6. Conditioning-selective synaptic alterations are not observed in neurons activated on S1 and S11

(A) No differences in AMPAR/NMDAR ratios between GFP+ and GFP– neurons in S1 in Paired and Unpaired mice (Paired; GFP+ n=6/8, GFP– n=4/5 Unpaired; GFP+ n=4/5, GFP– n=5/5). Decreased AMPAR/NMDAR ratios in GFP+ neurons in S11 in Paired and Unpaired mice (Paired; GFP+ n=5/5, GFP– n=6/7), Unpaired; GFP+ n=4/5, GFP– n=6/6). *Above:* Representative traces of AMPA/NMDAR recordings from layer II/III dmPFC pyramidal cells. Scale bars 20 pA, 50 ms **(B)** No differences in the frequency of spontaneous excitatory post-synaptic potentials (sEPSCs) between GFP+ and GFP– neurons in S1 in Paired and Unpaired mice. Decreased sEPSC frequency in GFP+ neurons in S11 in Paired and Unpaired mice. *Above:* Representative images of sEPSC recordings at -65 mV. Scale bars 15 pA, 75 ms. *Below:* Cumulative probability plots of sEPSC frequency. **(C)** No differences in sEPSC amplitudes between GFP+ and GFP– neurons in S1 and S11. *Below:* Cumulative probability plots of sEPSC amplitudes. (S1: Paired; GFP+ n=8/19, GFP– n=8/21, Unpaired; GFP+ n=8/18, GFP– n=8/19, Session 11: Paired; GFP+ n=8/20, GFP– n=8/24, Unpaired; GFP+ n=7/19, GFP– n=7/17). **(D)** No differences in Paired Pulse Ratios (PPR) of GFP+ and GFP– neurons in S1 and S11. (Paired; GFP+ n=7/8, GFP– n=7/9, Unpaired; GFP+ n=4/6, GFP– n=5/7, S11: Paired; GFP+ n=8/9, GFP– n=7/7, Unpaired; GFP+ n=7/7, GFP– n=6/6). All data are expressed as Mean±SEM; n= number of animals/number of cells total. **indicates main effect of Cell Type in a Two-way ANOVA P<0.05.*

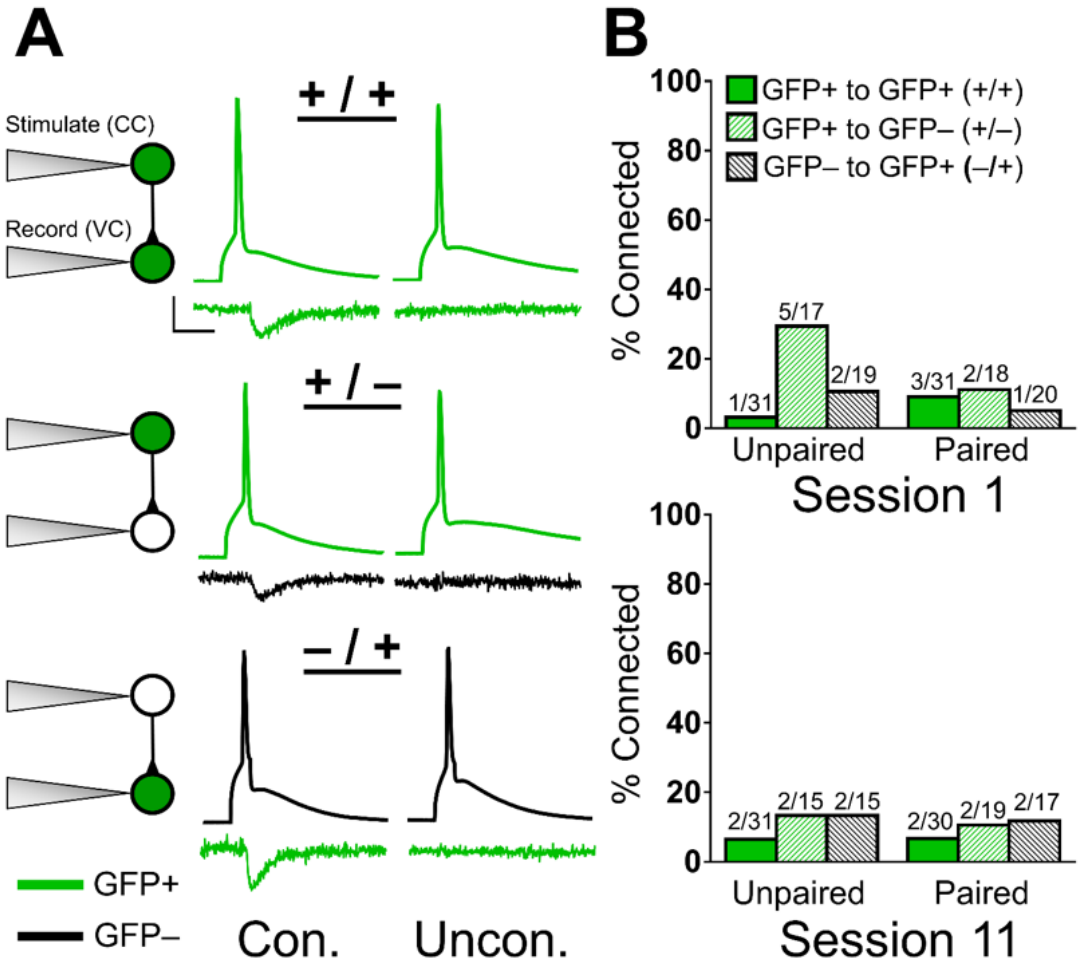
A
Stimulate (CC)
Record (VC)
+ / +
+ / –
– / +
GFP+
GFP–
Con.
Uncon.
B
GFP+ to GFP+ (+/+)
GFP+ to GFP– (+/–)
GFP– to GFP+ (–/+)
% Connected
100
80
60
40
20
0
1/31
5/17
2/19
3/31
2/18
1/20
Unpaired
Paired
Session 1
2/31
2/15
2/15
2/30
2/19
2/17
Session 11

Figure 7

Figure 7. No connectivity differences between GFP+ neurons and between GFP+ and GFP– neurons across Paired and Unpaired groups in S1 and S11. (A) Representative traces of connected (Con.) and unconnected (Uncon.) pairs recorded from a GFP+ to GFP+ neuron (+/+), GFP+ to GFP– neuron (+/–) and GFP– to GFP+ neuron (–/+). Neurons were stimulated in current clamp (CC) and postsynaptic excitatory currents recorded in voltage clamp (VC). Scale bar*:* 25 mV (CC)/ 25 pA (VC), 10 ms. (**B)** Percentage of +/+, +/– and –/+ connections in Paired and Unpaired mice from S1 and S11. There were no significant alterations in connectivity between groups.

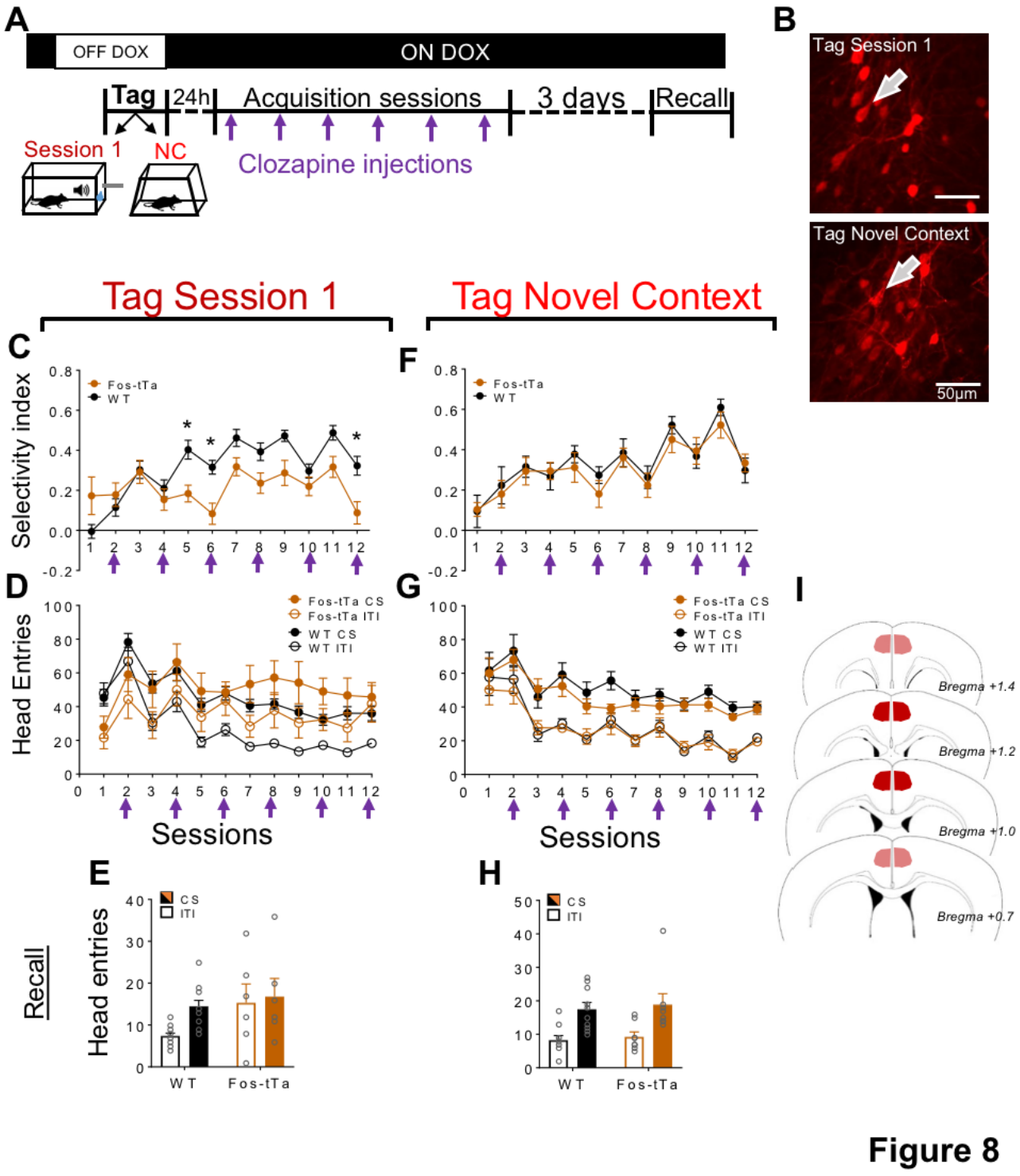
A
OFF DOX
ON DOX
Tag
24h
Acquisition sessions
3 days
Recall
Session 1
NC
Clozapine injections
B
Tag Session 1
Tag Novel Context
50µm
Tag Session 1
Tag Novel Context
C
Selectivity index
Fos-tTa
WT
F
D
Head Entries
Fos-tTa CS
Fos-tTa ITI
WT CS
WT ITI
Sessions
G
I
Bregma +1.4
Bregma +1.2
Bregma +1.0
Bregma +0.7
Recall
E
Head entries
CS
ITI
WT
Fos-tTa
H

Figure 8

Figure 8: Persistently enhancing the excitability of S1-activated neurons impairs conditioning. **(A)** Timeline of tagging and conditioning. All mice received clozapine injections on sessions 2, 4, 6, 8, 10 and 12 (purple arrows). Doxycycline was presented in the drinking water of all mice at all times, with the exception of its removal 48h prior to the tagging session, which lasted until 1 h following the tagging session. **(B)** Representative image of mCherry staining in dmPFC of *Fos-tTa* mice tagged during S1 or by exposure to a Novel context (NC); arrows indicate hM3Dq+ neurons. **(C) & (F)** Selectivity index of responses (CS-ITI/total number head entries) during acquisition in *Fos-tTA* (hM3Dq+; orange) and WT (hM3Dq–; black) mice following S1 or NC tagging. **(D) & (G)** CS and ITI responses during Acquisition in *Fos-tTA* (hM3Dq+; orange) and WT (hM3Dq–; black) mice following S1 or NC tagging. **(E) & (H)** CS and ITI responses during recall in *Fos-tTA* (hM3Dq+; orange) and WT (hM3Dq–; black) mice following S1 or NC tagging. **(I)** Schematic representation of injection sites All data are expressed as Mean±SEM * *P<0.05; S1 tag=6, 12; NC tag: n=8, 10.*

Tables and legends

	Session 1 (S1)				**Session 11 (S11)**			
	Unpaired		Paired		Unpaired		Paired	
	GFP-	GFP+	GFP-	GFP+	GFP-	GFP+	GFP-	GFP+
Resting Vm (mV)	-69.35 ±0.96	-67.30 ±1.18	-68.73 ±0.69	-68.95 ±0.76	-66.75 ±0.71	-67.16 ±0.52	-68.42 ±0.82	-68.32 ±0.74
Rheobase (pA)	77.33 ±6.83	103.27 ±18.58	121.00 ±16.69	75.14***** ±8.24	82.57 ±14.37	79.20 ±5.36	86.71 ±8.46	91.37 ±10.26
Ri (MΩ)	160.38 ±9.20	151.10 ±14.11	138.48 ±13.81	193.82****** ±15.19	181.62 ±21.67	143.14 ±9.01	165.31 ±13.39	161.89 ±8.70
AP Peak (mV)	67.00 ±4.47	66.38 ±3.26	68.71 ±2.37	65.76 ±3.53	68.40 ±2.66	70.61 ±2.22	67.19 ±2.47	73.40 ±2.23
AP Half-Width (ms)	1.30 ±0.09	1.33 ±0.07	1.21 ±0.04	1.21 0.05	1.28 ±0.04	1.32 ±0.04	1.33 ±0.05	1.34 ±0.04
Threshold (mV)	-36.51 ±0.85	-36.06 ±1.47	-34.36 ±1.00	-36.57 ±0.94	-35.46 ±0.74	-36.43 ±0.77	-35.86 ±0.65	-38.39 ±0.54
fAHP (mV)	-3.01 ±0.40	-2.48 ±0.35	-3.33 ±0.42	-3.72 ±0.47	-4.10 ±0.52	-3.69 ±0.48	-2.01 ±0.30	-3.56***** ±0.42
mAHP (mV)	-11.12 ±0.68	-9.93 ±0.69	-11.91 ±0.54	-10.51 ±0.44	-11.54 ±0.86	-10.37 ±1.32	-9.39 ±0.63	-11.47 ±0.48

Table 1

Table 1. Passive and active membrane properties following S1 and S11. Electrophysiological properties of GFP+ and GFP– pyramidal cells from Paired and Unpaired mice across conditioning sessions. All data are expressed as mean±SEM. Liquid junction potential was − 13.7 mV and was not adjusted for. Spike characteristics were determined from a single action potential (AP); when a doublet was elicited the second spike was analysed. Input resistance was calculated from the slope of the I/V curve measured in response to 4 pA current steps ranging from −60 to 40 pA. Spike threshold was measured using the third differential with Mini Analysis software. The AP peak was calculated as the difference between the AP peak and AP threshold. Half-width was measured as the AP width at half-maximal spike. Post-spike fast and medium afterhyperpolarizations (fAHPs and mAHPs) were measured ~3 and ~40 ms following the AP threshold respectively, similar to Ishikawa et al., (2009). Sidak post-hoc tests between GFP+ and GFP– are indicated *P<0.05, **P<0.01.

	H2B-GFP			
	Unpaired		Paired	
	GFP-	GFP+	GFP-	GFP+
Resting Vm (mV)	-66.42 ±0.67	-68.19 ±1.00	-66.37 ±0.79	-66.63 ±0.56
Rheobase (pA)	76.92 ±3.63	76.57 ±4.47	77.00 ±6.52	67.38 ±4.43
Ri (MΩ)	177.11 ±9.04	200.33 ±7.57	195.55 ±9.74	216.52 ±9.22
AP Peak (mV)	63.38 ±2.27	58.62 ±2.55	62.09 ±2.24	61.44 ±3.19
AP Half-Width (ms)	1.36 ±0.05	1.30 ±0.05	1.42 ±0.04	1.34 0.05
Threshold (mV)	-34.62 ±0.64	-33.57 ±0.57	-34.64 ±0.54	-34.70 ±0.71
fAHP (mV)	-4.27 ±0.43	-3.87 ±0.48	-3.71 ±0.44	-4.36 ±0.50
mAHP (mV)	-12.62 ±0.85	-11.00 ±0.78	-12.75 ±1.07	-11.41 ±2.22

Table 2

Table 2. Passive and active membrane properties from TetTag H2B-GFP mice 3-7 d following S1. Electrophysiological properties of H2B-GFP+ and H2B-GFP– neurons from Paired and Unpaired mice. All data are expressed as mean±SEM.